BBA Bioenergetics: Special Issue on Retinal Proteins

Channelrhodopsin unchained:

Structure and mechanism of a light-gated cation channel

Victor A. Lorenz-Fonfria and Joachim Heberle*

Freie Universität Berlin, Experimental Molecular Biophysics, Arnimallee 14, 14195 Berlin.

*to whom correspondence should be addressed.
e-mail: joachim.heberle@fu-berlin.de
Tel.: +49-30-838-56161

Contents

1. Introduction
2. Function and general properties of ChR2
    - 2.1. Ion channel activity
    - 2.2. Proton pumping activity
3. Structure of the dark state
    - 3.1. Channelopsin
    - 3.2. The DC gate
    - 3.3. The retinal chromophore
4. The ChR2 photocycle
    - 4.1. The photocycle under single turnover conditions
        - 4.1.1. Photocurrents
        - 4.1.2. Spectroscopy
        - 4.1.3. Correlation of electrical and optical experiments
    - 4.2. The photocycle under continuous illumination
5. Structural information about ChR2 photointermediates
    - 5.1. Conformational changes in the channelopsin moiety
        - 5.1.1. Pre-gating
        - 5.1.2. On-gating
        - 5.1.3. Off-gating
    - 5.2. Conformational changes in the retinal
    - 5.3. Proton transfer steps
        - 5.3.1. Deprotonation of the retinal Schiff base
        - 5.3.2. Reprotonation of the retinal Schiff base
        - 5.3.3. Proton transfers linked to proton-pumping activity
    - 5.4. The photocycle of 13-*cis* retinal
6. Conclusions

Abstract

The new and vibrant field of optogenetics was founded by the seminal discovery of channelrhodopsin, the first light-gated cation channel. Despite the innumerous applications that have revolutionized neurophysiology, the functional mechanism is far from understood on the molecular level. An arsenal of biophysical techniques has been established in the last decades of research on microbial rhodopsins. However, application of these techniques is hampered by the duration and the complexity of the photoreaction of channelrhodopsin compared with other microbial rhodopsins. A particular interest in resolving the molecular mechanism lies in the structural changes that lead to channel opening and closure. Here, we review the current structural and mechanistic knowledge that has been accomplished by integrating the static structure provided by X-ray crystallography and electron microscopy with time-resolved spectroscopic and electrophysiological techniques. The dynamical reactions of the chromophore are effectively coupled to structural changes of the protein, as shown by ultrafast spectroscopy. The hierarchical sequence of structural changes in the protein backbone that spans the time range from 10^{-12} s to 10^{-3} s prepares the channel to open and, consequently, cations can pass. Proton transfer reactions that are associated with channel gating have been resolved. In particular, glutamate 253 and aspartic acid 156 were identified as proton acceptor and donor to the retinal Schiff base. The latter proton transfer is the critical determinant for channel closure. The proton pathway that eventually leads to proton pumping is also discussed.

Abbreviations

ASR, *Anabaena* sensory rhodopsin; BHK cells, baby hamster kidney cells; bR, *H. salinarum* bacteriorhodopsin; *Ca*ChR, *Chlamydomonas augustae* channelrhodopsin; ChR, channelrhodopsin; ChR1, ChR1 from *Chlamydomonas reinhardtii*, ChR2, ChR2 from *Chlamydomonas reinhardtii*; C1C2; ChR1-ChR2 chimera; *Cy*ChR, *Chlamydomonas* yellowstonensis channelrhodopsin; *Ds*ChR, *Dunaliellasalina* channelrhodopsin; FTIR, Fourier transform infrared; HeLa cells, Henrietta Lacks cells; HEK cells, human embryonic kidney cells; hR, *H. salinarum* halorhodopsin; MD, molecular dynamics; MM, molecular mechanics; *Mv*ChR, *Mesostigmaviride*ChR; QM, quantum mechanics; SB, Schiff base; sRII, sensory rhodopsin II; *Vc*ChR, *Volvoxcarteri* ChR; YFP, yellow fluorescent protein.

1. Introduction

Ion transport in living organisms is divided into active and passive, and the proteins responsible are known as transporters (pumps, exchanges, carriers, etc.) and channels [1, 2]. Ion channels are central to living organisms; they are involved in signal transduction processes and in the conduction of electrical signals. Specifically, they mediate the uncoupled downhill movement of cations and anions across biological membranes by transiently opening an ion conductance pathway, a process known as gating [3]. The ion pathway generally consists of a narrow water-filled pore formed by specific residues in the protein interior, through which ions can diffuse across the otherwise impermeable cell membrane. Channels can be classified by the way the gating process is triggered. Ligand-gated channels open when specific molecules bind to them; voltage-gated channels open in response to changes in the electric field across the membrane; and mechanosensitive channels open following pressure changes [4]. The functionality of ion channels is generally studied by electrophysiology techniques, by measuring the flow of changes through the membrane (current) under variable conditions [5, 6].

Channelrhodopsins (ChRs) are the first and so far unique light-gated ion channels known in nature [7]. Cation permeation by ChRs can be triggered fast, repetitively, reproducibly, and non-invasively by light, opening new ways of addressing fundamental aspects of channel on- and off-gating with unprecedented temporal and spatial resolution. The first identified ChRs were ChR1 [7] and ChR2 [8], naturally hosted by the eyespot of the unicellular alga *Chlamydomonas reinhardtii*. More recently, up to thirteen ChR sequences have been identified in other green algae, differing among each other mainly in cation selectivity, kinetics, light wavelength sensitivity, and light intensity sensitivity [9-12]. Upon illumination, ChRs transiently increase their conductance for a variety of monovalent and divalent cations, leading to depolarisation of the cell membrane in milliseconds. Such a property has made ChRs a versatile and valuable optogenetic tool to alter the membrane potential of a host cell, mostly to control neural activity [13].

In their native host, ChRs are photoreceptors, being part of the poorly understood molecular machinery that directs unicellular algae toward or away from light (phototaxis) to optimise photosynthetic growth [14]. ChR1 and ChR2 are supposed to directly mediate the photocurrents that induce membrane depolarisation of the eye spot of *C. reinhardtii* [14], but the mediation of a secondary channel cannot be discarded [15]. While both ChR1 and ChR2 are responsible for the phototactic responses (each responding to different light intensities), the photophobic response is dominated by ChR1 [16-18].

ChRs lack sequence homology to any other known ion channel. Instead, they belong to the family of microbial rhodopsins, also known as type I rhodopsins, comprising light-driven ion-pumps and photoreceptors in archaea, eubacteria, fungi and algae [19]. Microbial rhodopsins share a similar primary sequence for the apoprotein (known as opsin), and a characteristic seven transmembrane membrane fold (7-TM) with the retinal chromophore covalently linked to a conserved lysine to form a protonated Schiff base (SB) [20]. The primary step in all known microbial rhodopsins, bacteriorhodopsin (bR) being the paradigm, is the photo-induced isomerisation of retinal around the C_{13}═C_{14} bond of the retinal chromophore. In ChRs, retinal isomerisation eventually leads to channel opening, presumably *via* concerted structural and electrostatic changes that are yet to be defined.

This review focuses on the functional and structural dynamics of ChR2 from *C. reinhardtii*. Among all ChRs known so far, ChR2 is most widely used in optogenetic applications [11, 13]. The properties of ChR1 or ChRs from organisms other than *C. reinhardtii* are discussed only whenever relevant to ChR2. All along the text, we use ChR2 residue numbering for all ChR sequences, but use the original numbering for other microbial rhodopsins (e.g., bR). Some additional aspects of ChR2 and ChRs in general, such as their physiological role in the phototaxis of algae [14, 21, 22], the properties of variants and chimeras [23, 24], or applications in optogenetics [13], are not or are only obliquely treated here.

2. Function and general properties of ChR2

2.1. Ion channel activity

In their seminal work, Nagel *et al.* [8] showed that both full length ChR2 and a fragment (1–315) comprising only the transmembrane region produced identical photocurrents and a very similar current/voltage relationship. The channel function is therefore confined to the 7-TM region. The function of the soluble cytoplasmic domain (approximately 400 amino acids) remains unknown. A truncated ChR2 construct has been used as a *de facto* wild-type (WT) in posterior studies, with the occasional addition of a yellow fluorescent protein (YFP) sequence at the C-terminus to monitor expression levels and cellular localisation by fluorescence microscopy [25] or a His tag when ChR2 is expressed and purified from *Pichia pastoris* [26].

The channel activity of ChR2 is monitored in electrical measurements [8]. Well-defined conditions require expressing ChR2 in a host cell and holding the membrane potential (voltage-clamp) at a constant ionic composition of the medium. The resulting light-induced current, the photocurrent, gives a measure of the net flow of cations. ChR2 photocurrents have been recorded in many naturally light-insensitive cells, namely *Xenopus* oocytes, human embryonic kidney (HEK) cells, baby hamster kidney (BHK) cells, Henrietta Lacks (HeLa) cells, cultured neurons, etc., and their properties have been shown to be mostly insensitive to the host system used [8, 24, 27, 28]. The photocurrents, usually measured using light pulses of several hundreds of milliseconds in duration, show a reversal potential for symmetrical ion concentrations close to zero volts: they are passive and thus linked to ion permeation. Anions are not conducted [7, 8], but protons and a wide range of monovalent and divalent cations are [8]. The permeability for protons is at least 10^6-fold higher than for any other monovalent cation [8, 27, 29], while the permeability for divalent alkaline cations (e.g., Ca^{2+}) is 10–100 times lower than for monovalent alkali ones (e.g., Na^{+}) [27, 29]. We should note that although ChR1 was initially defined as a selective

proton channel [7], it was later shown to be permeable to other cations as well [14]. Despite the much higher proton permeability, at physiological pH and cation concentrations, a significant part of the current is carried by cations other than protons [27, 30].

As expected for a channel, the photocurrents modestly increase with temperature (activation energy of ~20 kJ/mol), suggesting that cation permeation in the open state in ChR1 and ChR2 is rate-limited by small barriers for ion diffusion and not by energetic protein conformational fluctuations [7, 31]. While the activation energy for channel opening has not been determined yet, it is ~65 kJ/mol for channel closure [7, 31], large enough to indicate a coupling with protein conformational changes. The intensity of the photocurrents is inversely related to the atomic radius for alkali and alkaline cations, suggesting that they traverse the narrower region of the pore (the selectivity filter) in a mostly dehydrated state [8]. The dependence of the photocurrent on alkali cations of different sizes was used to estimate an effective cation pore of ChR2, found to be ~6.2 Å in diameter, in between the pore diameter of voltage-activated Na^+ channels and the nicotinic acetylcholine receptor [8, 32]. The photocurrents as a function of Na^+ concentration showed no sign of saturation [33], but they did for guanidinium (K_m=82 mM [31]) and Ca^{2+} (K_m=18 mM [33]).

The curved photocurrent/voltage relationship of ChR2 is characteristic for an inward rectified channel [34], i.e., for the same membrane potential, the current is higher (and thus the resistance is lower) when the potential is negative and cations flow to the inside of the cell. Single-molecule properties, indirectly deduced by photocurrent fluctuations, indicate that the inward rectification of ChR2 is intrinsic to the single-channel conductance, and not simply the result of a higher fraction of open channels at negative potentials [31]. The photocurrent-voltage dependence of ChR2 for various conducted cations could be better modelled using a single re-oriented binding site for which all the conducted cations compete (a model akin to those of transporters [35, 36]), than by using electro-diffusion models more familiar to those for channels [27, 37]. Two putative cation-binding sites have been identified in the

dark state of ChR2 by molecular dynamics (MD) simulations [38], one on the extracellular side (close to residues S52, N56, and E97 in helices A and B) and the other on the cytoplasmic side (close to E82, E83, H134, H265, and R268 in helices B, C, and G).

The single-channel conductance of ChR2 was estimated to be 60 fS for Na^+ at -60 mV by analysis of photocurrent fluctuations [31]. Such conductance would translate to a maximum turnover of 2×10^4 Na^+/s per ChR2 molecule (a current of ~15 fA for a single channel), too low for single-molecule electrical recordings [8, 31]. Despite its widespread use in optogenetics, ChR2 is arguably one of the less efficient ion channels known. The estimated unitary conductance of ChR2 is lower than archetypical ion channels by a factor of $10–10^4$ [3, 39]. ChR2 cation turnover is only two times higher than that of the Cl/HCO_3^- exchanger [40], one of the fastest transporters. Thus, the efficiency of ChR2 lies in the grey area between channels and transporters.

It is worth noting that it is not only the microbial rhodopsin family that comprises both ion pumps and channels, but also the family of Cl^- channels and transporters (ClC) [41]. In the latter case, it was even shown that a Cl^-/H^+ exchanger could be converted into a passive channel for Cl^- by the substitution of only two key residues [42]. The resulting Cl^- flow was 4×10^4 ions/s, i.e., 100–1000 times smaller than the most efficient Cl^- channels of the ClC family [39], but in the order of cation permeation by ChR2. This and other examples illustrate the fuzzy barrier between transporters and channels [39, 43, 44].

2.2. Proton pumping activity

In addition to being a cation channel, ChR2 exhibits light-driven proton pumping activity, as shown from photocurrents in planar lipid membranes and in giant HEK cells devoid of any electrochemical gradient [31]. In giant HEK cells, the photocurrent

was outwardly directed, i.e., in the same direction as in bR [31]. Comparison of the photocurrent intensity elicited by proton pumping and by passive cation transport provided an estimate of 0.2–0.4 charges pumped per photocycle. Thus, the authors concluded that ChR2 was a leaky proton pump [31]. Later, transient absorbance changes of a pH-sensitive dye followed by a short laser flash were recorded and normalised to the fraction of photo-excited ChR2 [45], following a similar approach as used previously to deduce the proton stoichiometry in bR [46]. Calibration of the pH-sensitive dye response yielded a stoichiometry of 0.3±0.1 protons released/taken up from the bulk medium per photocycle turnover [45]. Some of the internal proton transfer reactions responsible for the putative outward proton-pumping of ChR2 were later unravelled by time-resolved infrared (IR) spectroscopy (*vide infra* and [47]).

The co-existence of cation channel and proton-pumping activities in a single protein might appear exotic but it is not a unique feature of ChR2. It is at least also displayed in some Cl^- channels, presumably Cl^-/H^+ exchangers in origin [39]. Also noteworthy is evidence pointing to an active role of the residual H^+-pumping of Cl^- channels in their gating mechanism [48], a connection that might exist in ChR2 as well (*vide infra* and [47]).

3. Structure of the dark state

3.1. Channelopsin

Structural information on ChR2 was initially derived from homology modelling studies based on microbial rhodopsins of known structure [28, 49-51]. ChRs show modest primary sequence homology to other rhodopsins [7, 52], but most of the 22 amino acids in direct contact with the retinal are conserved, making helices C–G relatively easy to align. On the contrary, helices A and B show a low sequence homology and contain a large number of charged residues, a feature that produced conflicting results among different groups about the starting and the end points of

helices A and B. To illustrate the ambiguities and limitations of homology modelling approaches for ChR2 helices A and B, the homologous residue to E90 in ChR2 was assigned in bR to either L48 [28, 50], L62 [52], I45 [53], T46/L48 [51], or P50/Y43 [49] in helix B, or even to be located in the B–C loop [16]. A recent structure-based alignment of a ChR chimera with bR and other microbial rhodopsins set A53 of bR as the structural homologue to E90 in ChR2 [54].

The 6-Å projection map of two-dimensional (2D) crystals of ChR2 provided the first experimental confirmation of the otherwise expected 7-TM arrangement of ChR2 [55]. The projection maps resolved by electron crystallography on the C128T variant correlated well with previous results from bR [56], allowing the assignment of the transmembrane helices. ChR2 forms a dimer with protomers, interacting through helices C and D. The formation of a stable dimer by ChR2 was also indicated in previous experiments [57] but the functional relevance of this arrangement, if any, remains unclear.

The first and so far unique atomic structure of a ChR was published in 2012 by the group of Nureki [54]. A chimeric ChR was constructed by linking the last two helices (F and G) of ChR2 to the first five (A to E) of ChR1 with some additional modifications in the C-terminus, and named C1C2. Crystals were grown in darkness and the structure was resolved by X-ray crystallography to a resolution of 2.3 Å [54]. The high-resolution structure confirmed the dimeric arrangement observed in the 2D crystals of ChR2 [55]. Notably, C27, C34, and C36 in the N-termini form inter-protomer disulphide bonds [54], which were later shown to be only accessory for dimerisation [58, 59]. The C1C2 structure, depicted in Fig. 1a, is typical to microbial rhodopsins, especially for helices C–G. A distinct feature is the length of helix G, which extends 18 Å into the intracellular space. Yet, the most striking differences lie in helices A and B. These are tilted outward by 3–4 Å with respect to the bR structure, which leads to a cavity towards the extracellular medium and surrounded by helices A, B, C, and G (see Figs. 1a,b).

The surface potential of C1C2 shows that the cavity between helices A, B, C, and G forms an intruding electronegative pore, a half channel, rich in charged and polar residues mostly contributed by amino acids of helix B [54]. This helix contains five Glu residues, E82, E83, E90, E97, and E101 (Fig. 1b). From these five, E90 was shown to be protonated [60]. According to empirical pK_a calculations on the C1C2 structure, E82 and E101 might be ionic, whereas E83 and E97 are protonated at neutral pH [54, 61]. The cavity was concluded to form part of the pathway for cation permeation [54]. The putative cation-conducting pathway is opened towards the extracellular side but the cytoplasmic side is occluded, as expected for the non-conductive dark state. Two main constriction sites have been identified. The first is formed by S63 (helix A), E90 (helix B), and N258 (helix G), involved in a network of inter-helical H-bonds [54]. A stable H-bond between E90 and N258 has been confirmed in MD simulations, which also identified an inter-helical H-bond between E83 (helix B) and H134 (helix C) [62]. The latter residue corresponds to D96 in bR, where it acts as the SB proton donor [63, 64]. The second restriction is formed by the bulky side chain of Y70 in helix A [54]. The C1C2 X-structure shows that helices C and E are bent around T127-P129 and T188, respectively [54]. An intra-helical H-bond between the hydroxyl side chain (T127 and T188) and the carbonyl backbone (E123 and Y184) was proposed to contribute to the bending of these helices according to MD simulations [38]. The same work predicted an additional intra-helical H-bond in ChR2, involving T159-S155 and S155-G151 in helix D [38].

Electrophysiological experiments have shown that several point mutations alter the cation selectivity in ChR2 and in the C1C2 chimera, mostly for residues located in the glutamate-rich helix B (E90A/Q/H/K, K93A, E97A/K, E101K) but also in helices A (Q56A, Q56E, S63D), C (E123A, E123Q, L132C), and G (T250E, D253A, N258D) [28, 51, 53, 54, 65]. These mutations had an insignificant effect on the kinetics of the channel, and in most cases had a modest if any effect on the intensity of the photocurrents when taking into account uncertainties in the number of copies of functional protein in the cell membrane [28, 49, 54, 65]. ChR1 from *Mesostigma*

viride, *Mv*ChR1, lacks two of the five Glu residues present in helix B of ChR2 (E83 and E97), further supporting the idea that not all the Glu residues in helix B are essential for cation channel activity [9].

Among the tested variants in ChR2 and ChR1 and in the C1C2 chimera, only few mutations lead to an almost complete cessation of the photocurrents, namely: E97A (but not E97Q), R120A, H134D (but not H134R/Y/N), D253A/N (but not D253E), and H265R (but not H265A) [7, 28, 47, 49, 54, 65]. It is noteworthy that R120 and D253 are homologous to R82 and D212 in bR, two residues required for a native proton-pumping mechanism [63].

The crystal structure of C1C2 revealed the presence of β-sheet structures in the extracellular loop regions that might contribute to dimer stabilisation [54]. It also resolved six lipids and 43 water molecules per protomer [54]. MD simulations of structural models of ChR2 inferred a much larger number of internal water molecules than resolved in the X-ray structure, with water densities mostly clustered along the extracellular domain of helix B [38, 49]. Numerous water molecules were also predicted in the cytoplasmic domain, near E82, E83, H134, H265, and R268 [38, 49], with a water distribution discontinuity around E90 and S63 [38]. The environment of E90, located roughly half way through the membrane, was suggested to be hydrophobic in the dark state [51].

3.2. The DC gate

Replacement of C128 or D156 leads to a 10^2- to 10^5-fold extended lifetime of the conducting state of ChR2, namely 200-fold for C128T, 5×10^3-fold for C128A, 10^4-fold C128S, 5×10^4-fold for D156A, and 10^5-fold for the double mutant C128S/D156A [13, 66, 67]. Both residues are conserved in all known ChRs [9]. Fourier transform infrared (FTIR) difference spectroscopy experiments have shown that the carboxylic side chain of D156 is protonated and H-bonded in the dark-state, with a νC=O

frequency sensitive to the replacement of C128 [68]. It has been concluded that C128 and D156 side chains form a structural motif [66, 68], similarly to the homologous residues T90 and D115 in bR [69, 70]. The H-bond interaction connecting helices C and D (illustrated in Fig. 1c) was named the DC gate due to its functional relevance in the kinetics of channel closure [68].

This interaction was not confirmed by the crystallographic model of the C1C2 chimera [54]. The shortest distance between the terminal sulphur of C128 and the terminal oxygen atoms of D156 is 4.4 Å, a distance considered too large to support an H-bond [54]. It has been suggested instead that the S–H group interacts with the conjugated π-electron system of the retinal while the D156 side chain lacks any H-bond donor/acceptor [54]. The latter proposal is in direct conflict with the observed νC=O frequency of D156 at 1737 cm^{-1} in ChR2 [68], typical for a carboxylic group with one H-bond [71, 72]. At this point, it should be noted that helices C and D in the C1C2 chimera were derived from ChR1 and not from ChR2. *Acetabularia* rhodopsin II, a eukaryotic microbial rhodopsin, shows an H-bond between Asp92 and C218 of presumable functional importance [73]. The shortest distance between the oxygen and sulphur atoms of both side chains is 3.9 Å, suggesting that an H-bond between D156 and C128 in C1C2 cannot be fully ruled out. We also note that thiol and carboxylate groups, and to a lesser extent carboxylic groups, are prime candidates for chemical alterations induced by exposure to X-ray radiation [74, 75], even though the C1C2 structure did not show signs of radiation damage. Remarkably, neither C128 nor D156 displayed a stable conformation in MD simulations of the C1C2 chimera structure [62], which might indicate a shortcoming of the C1C2 structural model for these two side chains.

The functional importance of the DC gate in controlling channel closing kinetics has been questioned as well [38]. It was argued that if the phenotype of the C128 and D156 variants was solely ascribed to disruption to the DC gate, similar alterations in the channel closing kinetics for C128A and D156A variants were expected, while channel closing was ~10 times slower in the latter [13, 66, 67]. The

similarly retarded channel closing kinetics for C128A and C128S, the latter potentially able to form an H-bond with D156, was interpreted as evidence that the phenotype of C128 variants was caused by an influence of the sulphur in retinal re-isomerisation kinetics [67], although this left the effect of the D156A mutation unexplained. Recently, we could rationalise most of the similarities and differences in the phenotypes of C128 and D156 variants, after identifying D156 as the SB proton donor (*vide infra* and [47]).

Although the existence and functional relevance of the DC gate is well supported, the nature of the H-bond between C128 and D156 is still an open issue. The side chains of a cysteine and an aspartic acid can form an H-bond in two configurations: the oxygen atom of the C=O side chain of aspartic acid can act as the proton acceptor and the S-H of cysteine can work as an H-donor (type I), or the sulphur atom of cysteine can act as an H-acceptor and the O-H of aspartic acid can work as an H-donor (type II), as illustrated in Fig. 1c. It was initially suggested that C128 and D156 formed a type-I interaction [68]. Posterior MD simulations of a homology model of ChR2 built from *Anabaena* sensory rhodopsin (ASR) proposed instead a type-II interaction for C128 and D156 [49]. Energy calculations indicate that a type-II interaction is energetically favoured over a type-I interaction in a vacuum [71]. The calculated C=O stretching of a carboxylic group H-bonded to a cysteine is 1759 and 1747 cm^{-1} for a type-I and type-II interaction, respectively [71], with the latter closer to the experimental value of 1737 cm^{-1}. In the case of bR, experimental [76] and theoretical [77] results are consistent with the O-H of D115 being the H-bond donor to the oxygen of T90 side chain. On the other hand, a recent statistical analysis of 500 high-resolution X-ray structures of soluble proteins concluded that sulphur atoms were poor H-bond acceptors but moderately good H-bond donors [78]. Cys sulphur was four times less frequently found to act as an H-bond acceptor than as an H-bond donor.

As a third alternative for the DC gate, Watanabe *et al.* [49] proposed that the side chain of D156 might interact with the backbone oxygen of C128 and not with the

sulphur of the side chain. Recently, the same group proposed another structural model for the DC gate [38], based on MD simulations of a ChR2 structure model using C1C2 as a template. They inferred a potential water molecule bridging C128 and D156 residues [38]. The νC=O vibration frequency of D156 was calculated as 1741 cm^{-1} in this arrangement [77], close to the experimental value of 1737 cm^{-1}. Nevertheless, a clear-cut resolution of the controversy about the structural identity of the DC gate might await experimental and theoretical analysis of the S-H stretching of C128 and the O-H stretching of internal water molecules in various mutants of the DC gate, or a high-resolution crystallographic structure for ChR2. Irrespective of the results, it is evident that the DC gate is highly relevant to the mechanism of ChR.

3.3. The retinal chromophore

The π-electron system of the retinal gives rise to an electronic transition ($S_0 \rightarrow S_1$) in the visible spectrum of light. The spectral characteristics of retinal absorption are mostly affected by the protonated state of the SB, the planarity of the conjugated π-system of the retinal, the distance of the protonated SB to the counter-ions, and in general by the electronic environment of the retinal [79, 80]. In ChR2, the absorption spectrum of the retinal shows a global maximum at roughly 470 nm (Fig. 1d), notably blue-shifted with respect to light-adapted bR (568 nm), but close to sensory rhodopsin II (sRII; 487 nm) [81]. The action spectrum of ChR2, the wavelength dependence of the photocurrent amplitude following a short laser flash, shows a maximum at 475 nm, which matches well with the absorption spectrum of the retinal [33]. A protonated SB was confirmed by resonance Raman spectroscopy by observing a frequency shift in the SB C=N stretching in D_2O [82], a fingerprint for a protonated SB [83].

The visible absorption spectrum of the retinal exhibits a fine structure, putatively arising from coupling of the $S_0 \rightarrow S_1$ electronic transition with the C=C stretchings of the retinal, a phenomenon first discussed for sRII from *Halobacterium salinarum* [84].

The major maxima in ChR2 are at 479 nm, 445 nm, and 415 nm, resolved by calculating the second derivative (Fig. 1d). The energy difference between these peaks is ~1650±150 cm^{-1}, coherent with the coupling to the C=C stretching vibrations of the retinal chromophore (*vide infra*). Thus, the purely electronic transition (v=0→v'=0) in ChR2 likely corresponds to the absorption band at 479 nm.

Information about the retinal conformation was derived from resonance Raman spectroscopy. The retinal in-phase C=C (ethylenic mode) of ground-state ChR2 was identified at 1551 cm^{-1} [82], correlating well with the retinal absorption maximum at ~470–480 nm, based on a well-established empirical inverse correlation between both [85]. The co-existence of two retinal isomers in the dark state was indicated by two overlapping bands assignable to the retinal ethylenic mode, resolved by curve-fitting at 1550 and 1557 cm^{-1} [82]. Similarly, ASR [86], halorhodopsin (hR) [87], and bR [88] show two main components for the in-phase C=C stretching, one from all-*trans,*15-*anti* and the other from 13-*cis,* 15-*syn* retinal, with the latter upshifted by 7–11 cm^{-1}. The retinal C-C stretching region of ChR2, known as the retinal fingerprint, revealed overlapping bands at 1208, 1200, 1183, 1172, and 1155 cm^{-1} [82]. In bR, the intensity of the band at 1200 cm^{-1} originates predominantly from the C_{14}-C_{15} stretching of all-*trans*,15-*anti* retinal [88], while the 1183 cm^{-1} does it from the C_{10}-C_{11}stretching of 13-*cis*,15-*syn* retinal [89], further pointing to a mixture of all-*trans* and 13-*cis* retinal in the ChR2 ground state. The spectral overlap, combined with the uneven scattering cross-section of C=C and C-C stretching modes for different retinal isomers prevented a straightforward spectral quantification, but retinal extraction followed by high pressure liquid chromatography (HPLC) indicated a 70:30 all-*trans*:13-*cis* ratio (Fig. 1e). Thus, all-*trans* retinal is the predominant but not the sole retinal isomer in ChR2 [82]. The Raman spectrum of ChR2 dark state, and thus the retinal isomeric composition, was invariant for ChR2 solubilised in detergent (dodecylmaltoside) or reconstituted in lipid (dimyristoylphosphatidylcholine), and hardly affected by pre-illumination (light-adaptation) [82]. We should note that the electron density of the retinal in the C1C2 chimera was modelled using a planar all-

trans retinal at full occupancy [54]. The identification of a mixture of all-*trans* and 13-*cis* retinal from electron densities is not an easy task, and requires a resolution of <2.0 Å, as in ASR [90].

In the X-ray structure of the C1C2 chimera, the oxygen atoms of E123 and D253 side chains are very close to the retinal SB nitrogen, 3.4 and 3.0 Å, respectively (shortest distance). They are located almost 1 Å closer to the SB than D85 and D212 in bR, a feature that was noted to stabilise the state S_0 and enlarge the electronic energy gap with respect to bR [54]. Indeed, quantum mechanics (QM) excitation energy calculations have shown that E123 and D253 have the largest electrostatic contribution in blue-shifting the retinal absorption of C1C2 [62], which agrees with the 20 nm red-shift observed in the E123T variant of ChR2 [91]. It was suggested from empirical pK_a calculations [54] and hybrid quantum mechanical molecular mechanical (QM/MM simulations [38] that E123 is neutral and D253 ionic in the C1C2 chimera, but ionic for wild-type ChR2 [38].

Only one water molecule (w619) was resolved near the SB in the crystallographic structure of C1C2, too remote (4.4 Å) to act as an H-bond acceptor for the SB proton [54]. On ChR2, it was concluded from resonance Raman spectroscopic experiments that the protonated SB was strongly H-bonded, likely to a nearby water molecule, on the basis of frequency and bandwidth sensitivity of the C=N stretching to D_2O exchange [82]. A similar prediction was made for bR based on the same arguments [92] and confirmed later when high-resolution structures became available [93]. In the case of bR, three water molecules are located near the retinal SB, with one of them (w402) being the H-bond acceptor to the protonated SB and H-donor to the ionic D85 and D212 residues [93]. A recent QM/MM refinement of the SB environment of a ChR2 model built using the C1C2 structure as a template inferred the presence of three water molecules near the SB, with one of them being the H-bond acceptor from the protonated SB, although with an overall arrangement different from the pentagonal cluster of bR [38].

The retinal absorption of ChR2 is pH-independent in the range of pH 4–9 [60]. ChR2 does not contain titratable groups in this range whose protonation state modulates the energy gap of the electronic transition of the retinal. The situation is different in other ChRs. The action spectrum of *Volvox carteri* ChR1/2 chimera(*Vc*ChR1/2) shifted from 470 to 484 nm upon lowering of the extracellular pH from 7.5 to 4 [94], suggesting a pH-dependent equilibrium between two dark states, differing in the protonation state of an amino acid accessible (at least) from the extracellular bulk medium. A similar behaviour is observed in ChR1, where Glu87 (Ala48 in ChR2) was identified as the protonation site responsible for the shift of the retinal λ_{max} from 470 to 500 nm as the pH is decreased [33].

4. The ChR2 photocycle

In microbial rhodopsins, the initial photo-isomerisation of retinal around the C_{13}=C_{14} bond, habitually from *trans* to *cis*, leads to a thermally driven reaction that eventually restores the initial C_{13}=C_{14} conformation [20, 95]. During this thermal relaxation back to the ground state, a limited number of quasi-stable intermediary states are transiently populated, a process referred to as the photocycle [96]. The populated intermediate states differ to some degree in the retinal environment/conformation, protein backbone conformation, protonation state of specific groups, etc. These alterations translate in many cases into observable spectral changes, as shown by innumerable studies for bR and other rhodopsins. In the case of the light-gated ion channel ChR2, the intermediates also drastically differ in their conductance for monovalent and divalent cations [8], a property that cannot be directly probed currently by spectroscopic methods but is typically followed in electrophysiological measurements. In a wide sense, understanding the mechanism of ChR2 reduces first to the identification, and later, to the characterisation of intermediates that constitute the photocycle, including the dynamics of their interconversion. Arguably, this information is best revealed by time-resolved methods

following a short blue laser flash (of nanoseconds length or shorter), leading to a single turnover of the photocycle. We will also review aspects of the ChR2 photocycle under continuous turnover conditions, which is of increased complexity.

4.1. The photocycle under single turnover conditions

4.1.1. Photocurrents

Transient photocurrents following blue laser flashes of 10-ns duration have been measured for ChR2 [8, 26] and for *Vc*ChR1/2, an accidental hybrid from *Vc*ChR1 and *Vc*ChR2 that is functionally related to ChR2 [94]. More recently photocurrents under single turnover conditions have been also collected for various ChRs [97]. Representative transient photocurrents for ChR2 at -80 mV and +80 mV are shown in Fig. 2a, reproducing previously published data from the Bamberg group [26]. At a holding potential of -80 mV, cations flow to the cell interior and a negative current is recorded, a process reversed when the potential is held at +80 mV. ChR2 remains impermeable to cations for around 100 μs after photo-excitation. The current rises with $\tau_{1/2}$=200 μs (channel on-gating), with a peak of maximum conductivity at 1–2 ms, and it decays back to zero (channel off-gating) with $\tau_{1/2}$=8–22 ms [26]. Thus, WT ChR2 remains in a conductive state for around two decades of time. While the timing for channel opening is voltage-independent, the closing is not, and it is two-fold accelerated when the membrane potential changes from 0 mV to -100 mV [26]. Similar values were also reported for *Vc*ChR1/2 [94].

The current remains basically at zero from 100 ms on, even though the initial dark state requires more than 10 s for full recovery [26, 60]. Clearly, the open state is followed by a proportionally long-lived closed state. It should be noted that neither the channel opening nor the closing follows a simple exponential decay, suggesting the presence of at least either two open states, or a single open state in equilibrium with

two closed states. Further evidence for the presence of two open states comes from experiments under continuous illumination (*vide infra*).

In ChR2, electrogenic events besides cation channelling, such as a change in movements within the protein, appear to have a negligible contribution to the recorded currents, with the exception of a fast and small outward current (<20 μs) that is not properly resolved [26]. The outward photocurrent increased largely in D253E, a variant with 50-fold faster SB deprotonation. Its intensity was basically unaffected by reversing the potential from -60 mV to 60 mV, and was suggested to be related to the proton transfer from the SB to the proton acceptor [47]. A fast positive current, with a reversal potential of over -200 mV, was clearly resolved in ChR1 from various algae when expressed in *Escherichia coli*, a host system that allows for a faster response to electrical changes than HEK cells do [97]. The rise of the fast positive current correlated well with SB deprotonation kinetics probed by flash photolysis at 390 nm and was assigned to a proton transfer from the SB to an outwardly located acceptor [97].

Some variants of ChR2 and the C1C2 chimera display some noteworthy kinetic alterations in the photocurrents. However, the photocurrents of these variants have been characterised under continuous illumination, where only information about the channel closure kinetics can be reasonably extrapolated to single turnover experiments. E123T, E123A, and E123Q (but not E123D) show a two-fold accelerated channel closure [91], with a decay time constant barely affected by voltage, at least for E123T [98]. As a result, it was suggested that E123 might play a role in voltage sensing [98]. K93A and T250E also display two-fold faster channel off-kinetics [28, 54]. On the other hand, the E97A, L132C, H134R, T159C, G224S, and N258D variants present a two- to six-fold delayed channel closure, 20-fold delayed in case of E82A [24, 28, 32, 54, 65, 98, 99]. However, far more dramatic are the already discussed alterations in C128X and D156A variants, with a 200- to 10^5-fold delayed channel closure [13, 66, 67, 100].

4.1.2. Spectroscopy

The well-documented sensitivity of the retinal absorption to conformation and to the surrounding environment has made time-resolved ultraviolet/visible (UV/vis) spectroscopy the prime spectroscopic method used to characterise the ChR2 photocycle (Fig. 2c), as reviewed elsewhere [101].

Femtosecond vis-pump/vis-probe experiments [102], but also vis-pump/IR-probe experiments [103], have shown that photo-excitation of the retinal leads to an excited state that decays with τ=400 fs to populate a hot (i.e., vibrationally excited) red-shifted electronic ground-state photoproduct. Next, vibrational relaxation, with τ=3 ps, leads to the formation of an early red-shifted K-like intermediate characteristic for microbial rhodopsins, with an absorption maximum at 510 nm and presumably 13-*cis* retinal conformation [102]. It was noted that formation of the K-like intermediate was slightly delayed at pH 4.0 and in the E123T variant compared with the WT at pH 7 (5 ps vs. 3 ps), but not affected in the E123D variant, suggesting that a negatively charged amino acid at position 123 might assist isomerisation around the C_{13}=C_{14} bond [104]. A relaxation between K-like states, with a slight spectral effect on the retinal absorption, occurs with τ=200 ps [102]. This transition was tentatively assigned to the relaxation of the twisted chromophore in concert with the large conformational changes in the protein backbone inferred at this stage [104]. However, recent vis-pump/IR-probe experiments have shown that this transition is silent to IR spectroscopy and thus not coupled to protein conformational changes, which occur instead soon after vibrational relaxation (τ=13 ps) [103]. Because the first thermally activated transition in the ChR2 photocycle occurs with τ=200 ps, the precursor intermediate can be trapped by illumination under cryogenic conditions. Indeed, light excitation at 80 K provides UV/vis and IR difference spectra [60, 105] very similar to those observed 100 ps after photo-excitation at room temperature [103], confirming that changes in the protein backbone vibrations occur in the early picoseconds.

Flash photolysis provided information in the subsequent time range of 40 ns–50 s [47, 94, 102], i.e., the relevant time range when the channel opens and closes (Fig. 2b). The first intermediate is a red-shifted intermediate, formed in less than 40 ns. It shows an absorption difference maximum at 510 nm but an absolute maximum at 500 nm; thus, it was termed P500 or P_1^{500} [94]. It appears that this P_1^{500} state does not fully correspond to the last red-shifted intermediate resolved in pump-probe experiments [102], as concluded from some dissimilarities in their IR spectra [47]. Therefore, several P_1^{500} states have to be assumed that differ in the conformation of the retinal and the surrounding protein moiety.

Within $\tau_{1/2}$=10 μs, P_1^{500} intensity decays as the absorbance at 390 nm rises. We should clarify at this point that the formation and decay of intermediates in ChR2 are in general multi-exponential, and are not properly described by a single time constant. Therefore, we prefer the use of half-life time, $\tau_{1/2}$, to describe rise and decay kinetics. Considering the absorption maximum of this intermediate, 390 nm, and in analogy to other rhodopsins, it has been concluded that the SB deprotonates, leading to the formation of an M-like intermediate, termed P_2^{390} [26, 94]. D253 was suggested as the SB proton acceptor group by structural and functional data [54], but compelling evidence was provided by time-resolved FTIR studies [47], as will be explained below.

The decay of P_2^{390}, and thus SB reprotonation, proceeds with $\tau_{1/2}$=2 ms, concomitantly with the rise of a late red-shifted species absorbing at 520 nm, named P_3^{520}. The SB proton donor is D156 [47]. ChR2 releases protons to the medium in the early milliseconds, concurrent with the decay of P_2^{390} and the formation of P_3^{520} [45]. Thus, proton release is not temporally coupled to SB deprotonation as in bR, but coincides with SB reprotonation.

Although P_3^{520} decays with $\tau_{1/2}$=10 ms, the initial dark state is not fully recovered until much later. The P_4^{480} intermediate, spectrally similar to the ground state, forms with $\tau_{1/2}$=10 ms. Relaxation of P_4^{480} to the ground state is unusually slow for a

retinylidene protein, taking place with $\tau_{1/2}$=20 s. The kinetics of proton uptake from the medium is bi-phasic, following both P_3^{520} and P_4^{480} decay, and thus expand by more than three orders of magnitude [45]. It was unclear from UV/vis spectroscopy if the formation and decay of P_4^{480} were the last step of a linear photocycle or if they were the result of a branched reaction [26]. Recent results from time-resolved FTIR spectroscopy support the notion that P_4^{480} is a side path of the main photocycle, only transited by 25% of the ChR2 molecules [47]. The kinetics of dark state recovery from P_4^{480} appear to be pH-sensitive, and thus are thought to involve a pH-dependent equilibrium between two P_4^{480} intermediates, named $P480_a$ and $P480_b$ [60].

It was first noted by Bamann *et al*. [26] that the number of exponential terms needed to describe the ChR2 photocycle exceeded the number of spectrally different intermediates. Flash photolysis experiments of ChR2 from 10 ^{o}C to 30 ^{o}C consistently required six exponentials to describe kinetics longer than 1 μs [102]. Our own results suggest that eight exponential components are required to describe kinetics starting at 6 μs [47]. This implies that at least eight intermediate states are present in the ChR2 photocycle even though only four intermediates have been spectrally identified. The discrepancy might arise from the presence of substates, i.e., intermediates that cannot be easily discriminated due to their very similar spectral properties.

4.1.3. Correlation of electrical and optical experiments

The kinetics of the photocurrents can be related to the kinetics of the photocycle by flash photolysis. The open channel can be attributed to an intermediate of the photocycle, with a lifetime decay of ~10 ms, i.e., P_3^{520} decay is concurrent with channel closing or off-gating [26, 94]. Deprotonation of the SB (10 μs) precedes channel opening (200 μs), and thus cannot be the final necessary event for channel opening or the on-gating mechanism of ChR2 [26]. Channel opening occurs significantly earlier than P_3^{520} formation (~2 ms), i.e., it does not clearly correlate to

an intermediate as sensed by the retinal, and thus it might take place in the transition between two P_2^{390} substates. However, it cannot be completely ruled out that some of the observed differences in time constants are due to the different environment of ChR2 in electrical and optical experiments. The latter are conducted on purified ChR2 solubilised in detergent or reconstituted in lipids, which incidentally do not show essential differences among them [51, 82, 100]. Electrophysiological experiments are performed on ChR2 incorporated in a complex alien cell membrane and subjected to a controlled membrane voltage and chemical gradient [8]. While it is feasible to perform light-induced FTIR difference spectroscopy of a membrane protein under an applied voltage by means of surface-enhanced IR spectroscopy [106], this technique has not yet been optimised for time-resolved applications. Spectroscopic studies have been presented neither using asymmetrical pH values nor cation concentrations, conditions common in electrical experiments on ChR2 [8].

Kinetically independent evidence for an open state consisting of both P_2^{390} and P_3^{520} intermediates came from studies on the D156A and C128T variants [66]. Both display long-lived open states and similarly intense photocurrents, although the former presents mostly a long-lived P_2^{390} state and the latter predominantly a long-lived P_3^{520} state [66, 100]. In addition, both green and violet light were shown to effectively quench the currents, suggesting that both a blue-shifted (i.e., P_2^{390}) intermediate and a red-shifted (i.e., P_3^{520}) intermediate contribute to the cation conductivity. A fast equilibrium between a nonconductive P_2^{390} and a conductive P_3^{520} could not be discarded as an alternative explanation, however [66]. The on-gating mechanism in ChR2 appears to be spectroscopically silent in the UV/Vis region and, thus, it is likely to occur within P_2^{390} substates. This conclusion is consistent with findings from other rhodopsins that when the retinal is deprotonated, the sensitivity of its electronic transition to its environment is largely reduced, leading to optically silent transitions. Indirect evidence for P_3^{520} substates was observed in C128X variants. Unlike in WT, channel closure in these variants precedes P_3^{520} decay by around one order of magnitude [66, 100]. This observation was explained by two consecutive

P_3^{520} substates of which only the early one was conducting [100]. In summary, diverse evidence indicate that P_2^{390} and P_3^{520} intermediates, or at least some substates of them, represent open states of the channel.

4.2. The photocycle under continuous illumination

The photocycle of ChR2 increases in complexity under stationary light conditions. Not only do some of the time constants become dependent on light intensity [107], but most importantly, continuous illumination adds unwanted complications from secondary photoreactions. It is well known that photointermediates of retinal proteins exhibit their own photochemistry [108]. Photo-excitation of an intermediate might induce its photo-conversion to the ground state. For instance, it was shown for ChR2 [26] and C128X variants [66, 67] that channel closing is accelerated by green light pulses, presumably exciting P_3^{520} back to the ground state, as suggested by the subsequent increase in P_2^{390} formation seen for C128A [66]. In addition, violet light was shown to quench the stationary current in C128X and D156A variants, i.e., the channel is closed by photo-excitation of P_2^{390} [66], presumably back to the ground state, in analogy to the shunt of the M intermediate in bR [109]. Photo-excitation of intermediates can also initiate a new photocycle out of the main photocycle. Indeed, photoreaction of a late intermediate of the C128T variant leads to at least two non-native and long-lived inactive states, termed P380 and P353 [100]. These intermediates are closely related to free all-*trans* retinal, according to resonance Raman experiments, suggesting transient hydrolysis of the SB [110].

A peculiar feature of the photocurrents under continuous illumination is desensitisation, which is not observed in single turnover experiments. A few milliseconds after the illumination starts, the photocurrent typically reaches a peak that decays within some tens of milliseconds to a steady level (Fig. 3a). Desensitisation, also referred to as inactivation in the ChR2 literature, seemingly originates from ChR2 being temporally in a late low conductive state [107] and/or in a

mixture of conductive/non-conductive states, with the non-conductive state likely corresponding to P_4^{480} [94]. Desensitisation is often quantified by the ratio of the steady current to the peak current, which can be as low as 0.2–0.4 for ChR2 [29, 91, 98, 99]. The desensitised fraction increases with illumination intensity, and as the holding potential becomes more positive. It is reduced at low extracellular pH [33] and in some ChR2 variants [24, 51, 65]. Channel desensitisation is almost absent in ChR1 and in some ChR1-ChR2 chimeras [12, 24].

The photocurrents under continuous illumination suffer from an additional phenomenon known as light adaptation (Fig. 3a). It consists of the progressive reduction of the transient peak currents with repetitive periods of illumination, but without altering the intensity of the stationary current [8]. The full size of the peak photocurrents recovers after incubation in the dark, with $\tau_{1/2} \approx 5$–10 s [24, 26, 91], in a complementary process referred to as dark adaptation, which correlates well with the decay of P_4^{480} [26].

The relatively long time for dark adaptation together with channel desensitisation limit the applicability of ChR2 as an optogenetic tool [13]. Nevertheless, these two processes may be physiologically relevant to modulate the response of ChRs to light; for instance, to prevent full membrane depolarisation by attenuating or even inhibiting cation permeation under strong continuous illumination [111].

We should clarify that the terms light and dark adaptation as used in ChRs should not to be confused with a process known in microbial rhodopsins as dark/light adaptation. There, dark/light adaptation indicates differences in the isomeric composition of the retinal between pre-illuminated and dark-incubated ground states caused by a very slow (in relation to the time scale of the photocycle) thermal equilibration of the isomeric state of the retinal in the dark. In the case of bR, the dark-adapted form comprises a mixture of all-*trans*, 15-*anti* and 13-*cis*, 15-*syn* retinal, while the light-adapted form holds solely all-*trans*, 15-*anti* retinal [112, 113]. This type of dark-light adaptation is not observed for ChR2 [82].

While a linear model, including branching, provides an adequate description of the ChR2 photocycle under single turnover conditions, additions are required for the description of the photocurrents under continuous illumination. Quantitative analysis of ChR2 photocurrents under illumination with various light intensities and different periods of dark were provided by Nikolic *et al*. [107], and before that by Hegemann *et al.* for ChR1 [114]. These two and subsequent studies [115, 116] agree in the conclusion that two photocycles with connected open states are required to quantitatively describe the experimental photocurrents (Fig. 3b). Their modelling favoured two parallel photocycles with at least one open/conductive state in each cycle (O1 and O2) and two parent closed states (C1 and C2). The open states O1 and O2 are reached by photo-excitation of the C1 and C2 states, and they decay thermally back to C1 and C2 in ~10 ms and ~40 ms, respectively. These two photocycles intercross, with a reversible thermal transition between O1 and O2 (~100 ms), and with an irreversible transition from C2 to C1 (~10 s), i.e., C1 represents the dark-adapted ground state and C2 the light-adapted ground state [107]. The O1 state has ~10–20 times higher conductivity than O2 and different cation selectivity [30], a feature that explains the current desensitisation with light duration as O1 relaxes to O2, and O2 concentration builds up [27, 107]. Based on this model, light adaptation reflects the higher accumulation of C2 with respect to C1 after illumination is switched off, and dark adaptation corresponds to the slow recovery of C1 from C2 in the dark [114].

The dark-adapted C1 and light-adapted C2 states introduced on the basis of electrical experiments have been related to ground states D470 and D480 (with λ_{max} at 470 and 480 nm, respectively) [100]. The difference in λ_{max} was assigned to the protonation state of an unknown group near the retinal for *Vc*ChR1/2 [94]. It was concluded from a recent HPLC analysis of the C128T variant of ChR2 that the dark-adapted C1 state contained predominantly all-*trans*, 15-*anti* retinal, while light-adapted C2 showed mainly 13-*cis*, 15-*syn* retinal [117]. Accordingly, the λ_{max} of the dark-adapted C1 and light-adapted C2 states was reassigned to 480 nm and 470 nm,

respectively, in order to be consistent with the λ_{max} shifts observed in other microbial rhodopsins between all-*trans*, 15-*anti* retinal and 13-*cis*, 15-*syn* retinal [86-88]. This assignment about the nature of the C1 and C2 states implies that the photocycles of all-*trans*, 15-*anti* retinal and 13-*cis*, 15-*syn* retinal are both functional [117], arguing against indirect physiological evidences that relate cation permeation solely to the all-*trans* photocycle [101]. It also suggests that both all-*trans* and 13-*cis* photocycles should lead to the formation of similar intermediate states, in contrast to accumulated experience from other microbial rhodopsins [118-120].

5. Structural information about ChR2 photointermediates

The first structural information about changes in ChR2 intermediates came from steady-state FTIR difference spectroscopy [60, 105]. Continuous illumination at 80 K led to an intermediate state [60] that was shown to correspond to the early K-like intermediate observed in pump-probe experiments at 100 ps after the excitation laser pulse [103]. Continuous illumination under ambient conditions (293 K) led to a photo-stationary mixture of late intermediates. These initial data, recorded under photo-stationary conditions, have been recently completed and expanded by time-resolved IR spectroscopy experiments [47, 51, 103].

5.1. Conformational changes in the channelopsin moiety

Light gating of ChR2 involves the conversion of the retinal isomerisation into conformational changes of the apoprotein that eventually lead to cation permeation across the membrane. As the dark state represents a closed non-conductive structure, the formation or enlargement of water-filled pores inside the protein to form a transient channel is prerequisite for cation permeation.

So far, IR difference spectroscopy has been the main source of information on structural changes during the ChR2 photocycle. Conformational and environmental

changes in the protein backbone are mainly reflected in frequency changes of the amide I vibrations (1700–1620 cm^{-1}), comprising predominantly the C═O stretching mode of the peptide backbone [121]. Structural changes are also reflected in the amide II vibrations of the protein backbone (1570–1510 cm^{-1}), a coupled mode of the C–N stretching and N–H in-plane bending vibrations of the peptide bond [121]. The latter changes are often obscured in difference spectra of rhodopsins, due to overlapping contributions of the ethylenic C=C vibrations of the retinal [122].

The application of other structurally sensitive techniques to characterise protein conformational changes in the photocycle of ChR2 is, at the time of this review, limited to two reports using electron paramagnetic resonance (EPR) spectroscopy [58, 59]. Pulsed electron double resonance (pELDOR) spectroscopy [123] provides distance information between spin label sites in the 1.8–6 nm range with sub-nm precision [124]. Changes in the mutual distance of the spin labels are determined with high accuracy when the protein undergoes conformational changes. pELDOR experiments of freeze-trapped illuminated spin-labelled mutants were performed to infer movements of helices B and F in the P_3^{510} [59] and P_4^{480} [58] intermediates (which will be discussed later).

5.1.1. Pre-gating

It came as a surprise when large light-induced difference bands in the amide I region of ChR2 were observed at 80 K [60, 105], namely, a strong negative band at 1665 cm^{-1} and additional side bands (1691, 1684, 1652, 1645, 1637, and 1624 cm^{-1}). The spectral changes in the amide I region were much larger than those observed in any other microbial and animal rhodopsins, as illustrated in Fig. 4. We note that significant contributions to the intensity at 1665 cm^{-1} by the νC=N of the retinal or from an amino acid side chain vibration have been discarded due to the insensitivity upon H/D exchange [60, 103].

A differential band was observed at 1742(+)/1735(-) cm^{-1} when illuminating ChR2 at 80 K (Fig. 4 and [105]), corresponding to weakening of the H-bonding of the D156 carboxylic group [68]. The sensitivity of D156 to retinal isomerisation at 80 K is coherent with the interaction of D156 with C128, the latter residue in van der Waals contact with the retinal [54]. In P_1^{500} (early microseconds), D156 shows a broad positive band from the C=O stretching at around 1765 cm^{-1} [47] which is blue-shifted by about 30 cm^{-1} with respect to the ground state. The large shift suggests an even weaker H-bonding of D156 with C128 in P_1^{500}. The strength of the H-bonding of D156 is partially recovered upon the formation of P_2^{390}, where the C=O stretching of D156 downshifts to 1745 cm^{-1} [47], but still ~10 cm^{-1} blue-shifted with respect to the ground state.

Time-resolved FTIR spectroscopy revealed a differential feature at 1728(+)/1717(-) cm^{-1} in the P_1^{500}, P_2^{390}, and P_3^{520} states, which vanished in the E90A variant [47]. Similar bands at 1730(+)/1718(-) cm^{-1} were observed under steady-state illumination at room temperature, and assigned to E90 with the E90Q variant [60]. Thus, these two bands arise from H-bonding changes of the carboxylic group of E90 [47, 60], a residue interacting with S63 and N297 [54].

The nature of the protein conformational changes responsible for the observed spectral changes in the amide I and carboxylic regions before the channel opens is yet to be understood. The νC=O changes of E90 and D156 support alterations in inter-helical contacts between helices A-B-G and C-D, respectively, possibly reporting a change of the relative geometry of these helices. The frequency of the intense negative amide I band (1665-2 cm^{-1}, depending on the time scale) is indeed compatible with changes in the conformation of amide groups involved in transmembrane helices [125, 126]. Recently, it has been pointed out that the strength of the transition dipole moment of the amide I vibration, related to the extinction coefficient, increases with delocalisation of the amide I modes between adjacent residues [127]. The negative band in the difference spectrum of ChR2 might report a reduced coupling between residues in transmembrane helices that accompanies

retinal photo-isomerisation induced by kinking of one or more α-helices. Alternatively, the negative band in the microsecond P_1^{500} at 1662 cm^{-1} is kinetically related to a positive band at 1635 cm^{-1} and, thus, is tentatively assigned to the elongation of β-strands present in either the cytoplasmic (CP) or the extracellular (EC) loops [47].

Whatever the molecular basis of the above-presented large structural alterations, it is clear that they are present prior to cation permeation and, therefore, prepare for channel opening. Channel on-gating was anticipated to involve additional structural changes acting on top of these [105].

5.1.2. On-gating

The onset of cation permeation, or on-gating, takes place in the transition between P_2^{390} substates, i.e., after SB deprotonation ($\tau_{1/2}$=10 μs) and prior to SB reprotonation ($\tau_{1/2}$=2 ms). Additional changes in the amide I region were observed to evolve with $\tau_{1/2}$=60 μs, reporting protein conformational changes that were potentially connected to the on-gating process [47]. These changes involved the appearance of a positive band at 1650 cm^{-1} and an increase of the intensity of the negative band at 1663 cm^{-1} [47], both assignable to α-helical structures based on their vibrational frequency [121, 126]. The time evolution of both bands was highly correlated and also correlated reasonably well with the photocurrents, all peaking at 1 ms [26, 47].

The bands at 1663(-) and 1650 cm^{-1}(+) were suggested to arise from a 13 cm^{-1} downshift of the amide I of transmembrane helices upon their hydration [47]. Coherent with the above assignment, a band upshift was observed in the range of amide II vibrations of α-helical structures, at 1561(+)/1541(–) cm^{-1} [47]. These two amide II difference bands could not be resolved in the P_2^{390} and P_3^{520} states where ion permeation occurred but in the P_4^{480} state, because the overlapping ethylenic vibrations of the retinal are substantially reduced in intensity only in this intermediate [47].

As a summary, bands at 1663(-)/1650(+) cm^{-1} and 1561(+)/1540(-) cm^{-1}were taken as an indication of transient access of bulk water to previously 'dry' regions of the transmembrane helices, an event that kinetically correlates with the onset of cation permeation. The hydration might report the formation of a continuous water-filled channel inside the protein, or at least the enlargement of pre-existing water-filled cavities. The large number of internal water molecules present in the dark state, as determined by MD simulations, is noteworthy [38, 49, 51]. The conformational change that allows water to diffuse in was suggested to involve the rotation of one or more transmembrane helices [47], but experimental evidence was lacking. Recently, pELDOR experiments on a ChR2 variant containing the C128T mutation measured inter- and intra-monomer distances between labelled residues C79 (helix B) and C208 (helix F) [59]. It was observed that the intracellular domain of helix B moved outward in the P_3^{510} intermediate, accompanied by smaller rearrangements in helix F [59]. In light of these results, it is plausible that the movement of helix B, being part of the putative cation channel, is a structural determinant that allows water influx and cation permeation.

5.1.3. Off-gating

Channel closure, or off-gating, correlates with P_3^{520} decay [26]. Therefore, it is relevant to first discuss what the products of this decay are. It was observed that the ground state recovered in two well-separated phases, with a major recovery phase (75%) concurrent with P_3^{520} decay [47]. The remaining ground-state recovery (25%) followed P_4^{480} decay. The most straightforward interpretation is that P_3^{520} decays predominantly directly to the initial ground state, and partially to the P_4^{480} state [47]. Channel off-gating is, therefore, mostly accomplished during ground-state recovery, i.e., by the reversal of all the conformational changes and the resetting of the initial protonation states. The extremely retarded off-gating of D156A and C128X variants

convincingly suggests that ground-state recovery, the main route for off-gating is, under native conditions, rate-limited by D156 reprotonation kinetics [47].

Since P_4^{480} is a non-conductive state [26], channel off-gating also accompanies the P_3^{520} to P_4^{480} transition. Because these two late intermediates display similar changes in the amide I region [47, 117], the off-gating in this case is not accompanied by reversal of the major structural changes in the protein. We infer that the channel structure remains structurally open in P_4^{480}, and that cation permeation at this stage is inhibited by some other means. Indeed, pELDOR experiments measuring inter- and intra-monomer distances between labelled residues C79 and C208 showed similar distance changes in P_3^{510} [59] and P_4^{480} [58], supporting the movement of helix B in both intermediates. In spite of their expected similar structure, the P_3^{520} (conductive) and P_4^{480} (desensitised) states differ at least in the protonation state of D156, the H-bonding strength of the DC gate, and the protonation state of E90 [47]. The first two adopt their ground-state configuration in P_4^{480}: D156 is protonated and its H-bonding with C128 is unperturbed, i.e., ground state-like. Restoration of the interaction between helices C and D is, thus, a potential contribution to channel off-gating in P_4^{480}. The other notable difference corresponds to E90, which is deprotonated in P_4^{480} [51] but not in any other intermediate [47]. The mutation of E90 has no or very modest effect on the kinetics of channel closing [54, 65], and no effect on the photocycle [53], unlike mutations of D156 and C128 [66, 67]. E90 modulates cation selectivity [51], along with other residues in helices A, B, C, and G (*vide supra*).

What is then the functional implication of the deprotonation of E90? We have conjectured that the deprotonation of E90 in P_4^{480} could lead to a transiently stronger interaction with N258 and S63, restraining the dynamics of the adjacent helices A, B, and G, and contribute energetically to the off-gating [47]. This interpretation is hypothetical, as experimental evaluation of H-bonding strength in carboxylate groups is very challenging. However, in its support, channel desensitisation is indeed largely reduced upon the mutation of E90 or by low pH [51, 53, 65], supporting a contribution

of E90 deprotonation in stabilising a low conductive or non-conductive P_4^{480} state. E90 could also work as a pH sensor, adapting ChR2 activity to the pH of the medium (either extracellular or intracellular, depending on yet to be defined E90 connectivity).

Because the ChR2 photocycle is branched, as the strongly bi-phasic ground-state recovery kinetics suggest, a question emerges: at which stage do the two branches split? We have suggested that branching occurs at the level of the P_3^{520} state [47], by a kinetic competition between direct ground-state recovery and P_4^{480} state formation. The branching might also precede P_3^{520} decay, for instance, at the level of P_1^{500}, as was proposed by Bamann *et al.* [66].

5.2. Conformational changes in the retinal

The FTIR difference spectrum of ChR2 at 80 K shows in the C-C stretching region bands at 1245(-), 1237(-), 1204(-), 1191(+), 1183(-), 1177(+), and 1155(+) cm^{-1} (see Fig. 4 and [60, 105]). Light-adapted bR shows similar bands when illuminated at 77 K: at 1255(-), 1202(-), 1194(+), and 1169(-) cm^{-1}, accompanied by weaker bands/shoulders at 1248, 1216(-), and 1185(+) cm^{-1} (see Fig. 4 and [122]). The C-C stretching modes of the retinal are coupled with CCH in-plane rocking vibrations, making them sensitive to the *cis-trans* conformation of both the C-C and the C=C bonds [88]. The similar frequencies of many of these bands in ChR2 and bR lead to the conclusion that retinal photo-isomerisation in ChR2 is likewise from all-*trans*, 15-*anti* (negative bands at 1245, 1237, 1204, and 1155 cm^{-1}) to a distorted 13-*cis*, 15-*anti* conformation (positive band at 1191 cm^{-1}) [60, 105]. The assignment of the bands at 1183(-) and 1177(+) cm^{-1}, not discussed in the original reports, might be indicative of 13-*cis*, 15-*syn* retinal photochemistry, as discussed later.

The 13-*cis* conformation of retinal is maintained at least until P_3^{520}, as was concluded from the analysis of resonance Raman measurements on the C128T variant under photo-stationary conditions [105]. Quite intriguingly, continuous

illumination followed by retinal extraction and subsequent HPLC analysis of the C128T variant indicated that the retinal isomeric composition was barely affected with respect to the ground state [100], i.e., both P_3^{520} and P_4^{480} would appear to contain all-*trans* retinal. These results were recently revised, showing that the fraction of all-*trans* retinal in C128T was indeed largely reduced following illumination (from 78% to 43–56%), a process accompanied by an increase of 13-*cis* and small amounts of 11-*cis* and 9-*cis* retinal [117]. Retinal extraction also revealed slow and complex dark reactions [117], a complication that might be due to the slow thermal relaxation of other photocycles populated under continuous illumination in this variant.

The isomeric composition of retinal in WT ChR2 did not change substantially after continuous illumination, a conclusion supported by both resonance Raman spectroscopy and chemical retinal extraction [82, 100]. To account for this result, it has been proposed that both all-*trans* to 13-*cis* and 13-*cis* to all-*trans* photoreactions could occur in parallel and compensate for each other to leave the isomeric composition unchanged [100, 111]. Such an explanation contradicts FTIR difference spectra, which indicate that the retinal undergoes mostly an all-*trans* to 13-*cis* isomerisation after photo-excitation [60, 105]. The contradiction could be solved if the intermediate predominantly accumulated under photo-stationary conditions in WT, P_4^{480}, contains no longer 13-*cis* but all-*trans* retinal. In this line, the P_3^{520} to P_4^{480} transition was hypothesised to involve retinal reisomerisation, in order to account for the dramatic effect of the mutation of C128, a residue proposed to be critical for an efficient reisomerisation of the retinal from 13-*cis* to all-*trans* [67].

The νC=N of the retinal ground state was observed at 1657 cm^{-1} in H_2O and at 1629 cm^{-1} in D_2O by resonance Raman spectroscopy [82]. In the early photoproduct, the νC=N was assigned to a band at 1608–1599 cm^{-1} in D_2O by pump/probe IR spectroscopy [103]. Consequently, the unusually strong H-bond of the retinal SB in ChR2 [82] is disrupted following retinal photo-isomerisation, as in bR. There, the SB transiently loses its H-bond acceptor after retinal photo-isomerisation, as deduced by

the shift of the SB νC=N from 1640 cm^{-1} in the ground state (1626 cm^{-1} in D_2O) to 1613–1609 cm^{-1} (1605 cm^{-1} in D_2O) in the K intermediate [122, 128].

5.3. Proton transfer steps

The SB deprotonates and reprotonates during the photocycle of ChR2 [26] and protons are transiently released to and taken up from the medium [45] (Fig. 5). Furthermore, ChR2 displays active proton pumping activity [31]. During the photoreaction of ChR2, several amino acids change their protonation state. Among them, Asp and Glu residues are major components in proton transfers in proteins, and in microbial rhodopsins in particular [129]. Their pK_a can be modulated by changes in the H-bonding/electrostatic interactions with surrounding molecules. Furthermore, they can be involved in H-bonding interactions that are key elements in proton transfer. The C=O stretching vibration of the COOH group of Asp and Glu oscillates in the frequency range of 1780–1690 cm^{-1} [71, 72]. The region above 1710 cm^{-1} is rather isolated from vibrations of the peptide bond and other amino acid side chains [130], facilitating the identification of protonation changes of Asp/Glu residues.

5.3.1. Deprotonation of the retinal Schiff base

Deprotonation of the SB initiates the first proton transfer step in microbial rhodopsins [63]. E123 is the homologous residue to D85 in bR [8]. The latter was identified as an acceptor of the SB proton [131]. Electrophysiological experiments on E123T/A mutants demonstrated that this residue was not required for ChR2 function [8, 91], but could not address its putative role as a SB proton acceptor. More recently, Kato *et al.* [54] proposed D253 (homologous to D212 in bR) as the SB proton acceptor in the chimeric C1C2. Thereafter, compelling evidence for D253 being the SB proton acceptor in ChR2 was provided by time-resolved FTIR difference spectroscopy [47]. A positive band from the C=O stretching of the SB proton

acceptor was inferred at 1696 cm^{-1} for WT, and clearly identified at 1715 cm^{-1} and at 1713 cm^{-1} in the E123T and D253E variants, respectively. E123 was discarded as the SB proton acceptor by the small spectral and kinetic alterations introduced by the E123T mutation. On the other hand, D253E displayed 50-fold faster SB deprotonation kinetics, reminiscent of the acceleration observed in the D85E variant of bR [132], and exhibited significant spectral alterations in spite of the conservative amino acid exchange [47]. The D253N variant did not display a band from the C=O stretching of the SB proton acceptor even though the SB deprotonated almost normally, indicating that E123 was not the SB proton acceptor, even in the absence of D253. Note that in bR, the deprotonation of the SB still occurs in the D85N variant, even though with delayed kinetics [133, 134].

The low frequency of the C=O stretching of protonated D253, at 1696 cm^{-1}, suggests either that the OH group of D253 interacts with a strong H-bond acceptor (e.g., a carboxylate group [135]), that the C=O group of D253 does it with a strong H-bond donor (e.g., NH_3^+ from a lysine [71, 72]), or both. On such basis, we have tentatively proposed that E123 forms a strong H-bond with D253 when the latter is protonated, an interaction that is weakened in the E123T and D253E variants [47]. A νC=O frequency of a carboxylic group of as low as 1719 and 1713 cm^{-1} was observed in the E194D and E204D variants of bR [136-138]. Both conditions correspond to a carboxylic group H-bonded to a carboxylate group, either directly [139] or indirectly, through a water molecule [137]. Accordingly to a recent dark-state model of ChR2 refined with QM/MM, D253 and E123 side chains would interact indirectly through two water molecules [38], making plausible a water-mediated interaction between both residues also when D253 is protonated. Protonated D212 in bR displays a C=O frequency of 1712 cm^{-1} [140-142], explained by a combination of H-bonds with two tyrosines (Y57 and Y185) and a water oxygen [143], illustrating that other arrangements of H-bond interactions can also produce a low C=O frequency for a Asp/Glu residue.

Different conclusions regarding the nature of the SB proton acceptor were drawn from the analysis of the photocurrents of *Chlamydomonas augustae* ChR1 (*Ca*ChR1) and *Vc*ChR1 [97]. Both showed a fast and intense outward photocurrent assigned to the proton transfer from the SB to the proton acceptor. The outward current was largely reduced in the E123Q variant but roughly preserved in D253N. Both variants displayed SB deprotonation. The authors concluded that E123 was the primary proton acceptor while D253 acted as an alternative proton acceptor in the absence of the former [97]. The A123E mutation of *Dunaliella salina* ChR1 (*Ds*ChR1) enhanced the fast outward photocurrents, indirectly suggesting that a Asp/Glu group at position 123 is the most efficient proton acceptor whenever present [97].

An acidic residue at position 253, but not at position 123, is conserved in the family of ChRs. In *Ds*ChR1, E123 is replaced by alanine, while D253 changes to glutamate [11]. Channel functionality is preserved upon neutralisation of E123 in ChR2 [91], C1C2 [54], *Ca*ChR1, as well as in *Vc*ChR1 [97], thus confirming that a protonable group at position 123 is not a functional requirement in ChRs. The replacement of D253 by non-protonable residues correlates with impaired functionality, as shown for D253A in C1C2 [54] and in *Ds*ChR [11], and for D253N in ChR2 [47], in *Ca*ChR1, and in *Vc*ChR1 [97]. The SB still deprotonates though, at least in the D253N variants [47, 97]. The conservative variants D253E [47] and E253D [11] in ChR2 and *Ds*ChR, respectively, retain the photocurrents. Therefore, it is concluded that transient protonation of the residue at position 253, rather than the SB deprotonation itself, is a prerequisite for functionality.

5.3.2. Reprotonation of the retinal Schiff base

The homologue residue to the SB proton donor D96 in bR is H134 in ChR2 [8]. In ChR1, the H134D replacement led to a loss of function, while H134R and H134Y exchanges preserved it [7]. The H134R/S in ChR2 variants led to preserved or even improved photocurrents [25, 37], whereas H134Y was barely functional [26]. Given

the unknown link between proton transfers and channel functionality, the above findings alone did not strictly discard H134 as the SB proton donor. It is noteworthy that a His at position 134 is conserved in most but not all ChRs [9]. In *Mv*ChR1, this His is replaced by an Ala, whose exchange to either His or Arg abolished the photocurrents [9]. More recently, E83 and E90 were also suggested to be candidates for the SB proton donor in C1C2, based on their spatial location and empirical pK_a calculations [54].

Contrary to these suggestions, we succeeded in identify D156 as the internal proton donor of the SB by means of time-resolved FTIR spectroscopy [47]. The SB proton donor in ChR2 corresponds to a carboxylic group with a C=O stretching at 1737 cm^{-1} in the ground state, a group that deprotonates concomitantly with SB reprotonation. The resulting negative band at 1737 cm^{-1} shifted to 1763 cm^{-1} in the D156E variant and vanished in D156A, but it was preserved in other variants (E90A, E123T, D253E, and D253N), supporting the assignment to D156 [47].

The identification of D156 as the SB proton donor provided the clue to explain the extremely long lifetime of the P_2^{390} intermediate observed for the D156A variant [66]. In the absence of a suitable internal proton donor, SB reprotonation is rate-limited by slow proton diffusion, presumably from the bulk and, thus, mutation of the SB proton donor extends the lifetime of the deprotonated SB. These results are reminiscent of the functional consequences of the D96N/A variants in bR [64], D108Q in proteorhodopsin [144], or E132Q in *Gloeobacter* rhodopsin [145]. We infer that the photocycle of D156A will be accelerated at low pH, as well as by small buffer molecules such as azide, much like D96N/A variants of bR [144, 146].

D156 in ChR2 corresponds to D115 in bR, a residue protonated during the entire photocycle [147] and only indirectly involved in the proton pump mechanism [148, 149]. Interestingly, the mutation of T90 in bR (the residue equivalent to C128 in ChR2) to Ala or Val turned D115 ionic in the ground state [70], i.e., T90A/V mutations largely reduce the pK_a of D115 in bR. We anticipate that the replacement of C128 will

reduce the pK_a (proton affinity) of D156 [47], explaining why C128X variants exhibited an extended lifetime of the P_3^{520} intermediate [66]. In the C128T variant, the slow decay of P_3^{520} was 10-fold accelerated at pH 6 in the presence of 30 mM azide [100], a small molecule known to facilitate proton transfers [150]. This observation is in line with the rate-limiting step for P_3^{520} decay in C128T being the reprotonation of a residue, presumably D156. We speculate that the pK_a of D156 is dropped sufficiently low in some C128 variants for D156 to be partially deprotonated in the ground state, as reported previously for D115 in bR in the T90A/V variants [70]. Indeed, a pH-dependent fraction of deprotonated D156 (i.e., inactive SB proton donor) qualitatively explains the otherwise puzzling observation that C128X variants show both long-lived P_2^{390} and P_3^{520} states, with a fraction of P_2^{390} decreasing with the bulk pH [66].

We finally point out that the T90A variant abolishes light adaptation in bR, i.e., the conversion of ground-state 13-cis, 15-*syn* to ground-state all-*trans*, 15-a*nti* retinal by illumination [151]. Such behaviour suggests that T90 is involved in the conversion between all-*trans*, 15-*anti* and 13-*cis*, 15-*syn* conformations of retinal. It is plausible that C128, but not D156, may play a similar role in ChR2. Such a feature can account for additional spectroscopic and kinetic differences between C128X and D156A variants.

5.3.3. Proton transfers linked to proton-pumping activity

We recently resolved proton transfer reactions in ChR2 [47]. The initial proton transfer takes place from the SB to D253 and proceeds with $\tau_{1/2}$=10μs. The SB reprotonates from D156 with $\tau_{1/2}$=2 ms. Concomitantly, a proton is released to the bulk, as deduced by transient pH changes monitored by a pH-sensitive dye [45]. The proton is released to the extracellular side, a reasonable assumption required to account for the outward proton-pumping activity of ChR2 [31]. The source of the released proton is not D253, which instead stays protonated at this stage. Thus, we infer the presence of a proton release group that is yet to be identified [47]. The

proton release group in bR involves E194, E204, and water molecules, as well as additional stabilising amino acids [152-154]. The equivalent groups to E194 and E204 in ChR2 are E235 and S245, respectively. Both residues are highly conserved in other ChRs, with the exception of *Ca*ChR1 and *Cy*ChR1, where they are replaced by S235 and D245, respectively [12]. The role of these residues, if any, remains unclear. While the mutation S245E did not affect the photocycle nor the proton release kinetics in ChR2 [45], it abolished the photocurrents in *Mv*ChR2 [12].

D156 is reprotonated with $\tau_{1/2}$=10 ms [47], concomitantly with proton uptake from the bulk [45]. Given the location of D156 in the intracellular domain of ChR2, we have proposed that D156 reprotonates from the intracellular medium [47], completing a series of proton transfers that account for the proton-pumping activity of ChR2 [31].

A fraction of ChR2, estimated to be 25–20% *(vide supra)*, undergo the P_3^{520} to P_4^{480} transition prior to ground-state recovery. This transition is accompanied by the deprotonation of E90 ($\tau_{1/2}$=10 ms), which is reprotonated upon P_4^{480} decay to the initial dark state ($\tau_{1/2}$=20 s). E90 deprotonation/reprotonation is to the aqueous bulk phase, as revealed by transient pH-change measurements with the E90A variant [47]. It is still to be defined if proton release and uptake from E90 is towards the cytoplasmic or the extracellular side of the membrane.

5.4. The photocycle of 13-*cis* retinal

While all-*trans* retinal is the predominant isomer in the dark state of ChR2, the contribution of the 13-*cis* photoreaction to the ChR2 photocycle remains elusive. Also, an open question is whether the 13-*cis* photocycle is involved in ChR2 function and, thus, contributes to the recorded photocurrents.

Heterogeneity in the photocycle caused by different retinal isomers can be deduced by kinetic changes when using different excitation wavelengths. In time-resolved UV/vis experiments on WT ChR2 and the C128T variant, the primary

isomerisation event and the successive kinetics of the photoproducts were not affected by the variation of the excitation wavelength [66, 102]. In support, the kinetics of the photocurrents also did not differ by the change in wavelength of the exciting laser flash [33], suggesting that a single ground state was associated with the photocurrents. In ASR, the quantum efficiency for retinal photoisomerisation is 40% for all-*trans* retinal but only 20% for 13-*cis* retinal [155]. If the same relative quantum efficiencies apply to ChR2, the photoproducts of 13-*cis* retinal would be barely accumulated and, thus, they would hardly contribute to the recorded data as the experiments above suggest. Alternatively, the above experiments might have failed in resolving contributions from the 13-*cis* photocycle from the similar λ_{max} values of all-*trans* and 13-*cis* retinal, which are supposed to differ by no more than 10 nm.

The light-induced IR difference spectrum of the photoreaction of 13-*cis*, 15-*syn* retinal of bR recorded at 77 K (K-BR_{13cis}) displayed a pair of bands at 1186(-) and 1179(+) cm^{-1} in the retinal fingerprint region [156]. The former band is characteristic for the C_{10}-C_{11}stretching of 13-*cis*, 15-*syn* retinal [89], while the latter band is considered a marker for the formation of a distorted all-*trans* photoproduct arising from the fraction of ground-state 13-*cis* retinal [156]. A similar pair of bands is observed for the photoreaction of 13-*cis* retinal in ASR [157]. Similar bands are discernible at 1183(-) and 1177(+) cm^{-1} for ChR2 (see Fig. 4 and [60, 68]). None of them, however, clearly correspond to the all-*trans* retinal photoreaction (see Fig. 4), but are akin to K-BR_{13cis}. The appearance of the 1183(-) and 1177(+) cm^{-1} bands suggests that photo-excitation of 13-*cis* retinal in ChR2 leads to the formation of an all-*trans* photoproduct that overlaps with the photoproduct from all-*trans* retinal. Thus, it appears that 13-*cis* retinal photoproducts do contribute to the ChR2 photoreaction. The question is whether the 13-*cis* photocycle is functionally relevant.

In dark-adapted bR, the 13-*cis* retinal shows a photocycle that mostly involves one or more long-lived red-shifted intermediate lacking the transient deprotonation of the SB (M formation) and, thus, is not coupled to proton pumping [119, 158]. SB

deprotonation and proton pumping were suggested to take place in the 13-*cis* photocycle only at high pH [159, 160]. For ASR, it was also concluded that SB deprotonation occurred solely, or at least predominantly, in the all-*trans* but not in the 13-*cis* photocycle [86]. It has been suggested that the *syn* conformation of the C=N bond in 13-*cis* retinal either places the SB in an incorrect orientation after photo-isomerisation [88, 161] or leads to an insufficient light-induced change in the pK_a of the SB to deprotonate [160]. Therefore, if D253 protonation from the SB and D156 reprotonation from the bulk are important events for channel opening and closure in ChR2, as they appear to be, it seems unlikely that the 13-*cis* photocycle of ChR2 bears any functional relevance.

6. Conclusions

The last decade has witnessed a burst of optogenetic applications in neurophysiology, based on the capacity of ChR to depolarise neuronal cells via remote illumination. Though less rapid, notable advances have recently been achieved in deciphering the functional mechanism of channelrhodopsin at the molecular level. In this last aspect, bR serves as a model. Indeed, many biophysical techniques established to unravel details of the photoreaction of bR have recently been applied to channelrhodopsin as well.

As complex as the molecular mechanism of bR might have appeared 40 years ago, the fact that the community worked on bR of a single origin (*H. salinarum,* for details see [162] and the review article by Grote, Engelhard, and Hegemann [163] in this volume) ensured a common ground to integrate results from different techniques. Since then, the situation has dramatically changed as sequencing came up with a diversity of proteins having the same or very similar functionality. Despite the same light-gated channel function, the plasticity of channelrhodopsins with varying amino acid sequences even at seemingly critical spatial positions (for details see review articles by Spudich, Sineshchekov and Govorunova [164] and by del Val et al. [165]

in this volume) renders the molecular mechanism difficult to resolve when results from channelrhodopsins of different origins are compared. The difficulty in understanding channelrhodopsins is enhanced by the fact that at least two different forms of the retinal chromophore (all-*trans* and 13-*cis* retinal) exist in the dark state of all channelrhodopsins examined so far.

Unique to channelrhodopsin is the mechanistic link between retinal isomerisation and channel gating (Fig. 5). Electrophysiological and spectroscopic experiments performed on WT and site-directed mutants of channelrhodopsin have provided hints to the relevance of proton relocations in gating (*vide supra*). However, central parameters in neurophysiology, such as the influence of membrane potential can be assessed at the molecular level only by merging electrophysiology and spectroscopy. Technical advances towards this goal have been achieved [106, 166-168] and the application to channelrhodopsin is underway.

It is evident that the level of structural information must be increased to be able to understand the functional mechanism of channelrhodopsin. In particular, the localisation of water molecules in the cation channel is of crucial relevance. Obtaining crystals of channelrhodopsin that diffract to a higher resolution will allow the identification of more water molecules than in the current structural model of the dark state [54]. Since only tightly bound water molecules are resolved by crystallography, complementary methods will be required to monitor weakly bound water molecules. Here, FTIR difference spectroscopy and MD simulations are the methods of choice (see articles by Furutani & Kandori [169] and by Gerwert, Freier, and Wolf [170] in this issue), which are also able to address the active involvement of water molecules in the reaction mechanism.

As most of the mechanistic details have been assessed using ChR2 from *C. reinhardtii* and ChR2 is the protein mostly employed in optogenetic applications, it is desirable to have the structure of the WT solved. Intermediate states are trapped by continuous illumination at specific temperatures due to the fact that the transitions of

the photocycle intermediates are thermally driven. However, a detailed protocol on the temperatures required to trap a specific state is still to be developed. Protein variants may also be helpful, where critical amino acid residues are exchanged to prolong the lifetime of specific intermediate states. Once the intermediate state has been trapped, X-ray crystallography or electron microscopy is applied to resolve the structure of these states in the three-dimensional (3D) or 2D crystals, respectively. However, the restraints imposed by the crystal lattice reduce the flexibility of the protein backbone and side chains. This effect is intended in crystal growth but may restrict conformational changes of the protein during catalytic activity, as has been demonstrated for other microbial rhodopsins [171, 172]. In this regard, fluorescence (see article by Alexiev & Farrens [173] in this volume) and EPR spectroscopy [58, 59] can measure distances between judiciously placed labels without the need of a crystal lattice.

All of these structural techniques provide only still pictures. Time-resolved structural data employing novel pulsed X-ray [174, 175] or electron sources [176, 177] will depict the dance of molecules involved in channel gating. In the end, theoretical approaches will determine the energy landscape as well as its change upon electronic excitation and thermal relaxation through the various intermediate states of the photocycle. By these means, a fundamental understanding of functionality will be achieved that answers not only the question ‘How does the machine work?’ but ‘Why?’

Acknowledgements

The fruitful collaboration with friends and colleagues (Ernst Bamberg, Christian Bamann, Josef Wachtveitl, Gabriele Fischer von Mollard, Cristiano Viappiani, and Robert Bittl) is gratefully acknowledged. We are thankful, in particular, to Christian Bamann (Max-Planck institute for Biophysics, Frankfurt) for providing the time-resolved photocurrent data and the chromatogram of retinal extraction from ChR2,

Melanie Hey (née Nack, FU Berlin) for the UV/Vis spectrum of ChR2, and Hideki Kandori (Nagoya Tech) for permission to reproduce the IR difference spectra of bR and bovine rhodopsin recorded at 77 K. We thank Dorothea Heinrich, Nils Krause, Ionela Radu, Tom Resler, Ramona Schlesinger, Bernd-Joachim Schultz, and Ingrid Wallat (Biophysics at the FU Berlin) who contributed to the presented results at various stages. This work was supported by grants from the Deutsche Forschungsgemeinschaft to J.H. (FOR-1279, SFB-1078, B3).

References

[1] E. Gouaux, R. Mackinnon, Principles of selective ion transport in channels and pumps, Science 310 (2005) 1461-1465.
[2] G.R. Dubyak, Ion homeostasis, channels, and transporters: an update on cellular mechanisms, Adv. Physiol. Educ. 28 (2004) 143-154.
[3] F. Tombola, M.M. Pathak, E.Y. Isacoff, How does voltage open an ion channel?, Annu. Rev. Cell. Dev. Biol. 22 (2006) 23-52.
[4] B. Corry, S.H. Chung, Mechanisms of valence selectivity in biological ion channels, Cell. Mol. Life Sci. 63 (2006) 301-315.
[5] B. Hille, Ion Channels of Excitable Membranes, third ed., Sinauer Associates INC, 2001.
[6] M. Carter, J. Shieh, Guide to Research Techniques in Neuroscience, first ed., Academic Press, Elsevier Inc, London, 2010.
[7] G. Nagel, D. Ollig, M. Fuhrmann, S. Kateriya, A.M. Musti, E. Bamberg, P. Hegemann, Channelrhodopsin-1: a light-gated proton channel in green algae, Science 296 (2002) 2395-2398.
[8] G. Nagel, T. Szellas, W. Huhn, S. Kateriya, N. Adeishvili, P. Berthold, D. Ollig, P. Hegemann, E. Bamberg, Channelrhodopsin-2, a directly light-gated cation-selective membrane channel, Proc. Natl. Acad. Sci U. S. A. 100 (2003) 13940-13945.
[9] E.G. Govorunova, E.N. Spudich, C.E. Lane, O.A. Sineshchekov, J.L. Spudich, New channelrhodopsin with a red-shifted spectrum and rapid kinetics from *Mesostigma viride*, MBio 2 (2011) e00115-00111.
[10] F. Zhang, M. Prigge, F. Beyrière, S.P. Tsunoda, J. Mattis, O. Yizhar, P. Hegemann, K. Deisseroth, Red-shifted optogenetic excitation: a tool for fast neural control derived from *Volvox carteri*, Nat. Neurosci. 11 (2008) 631-633.
[11] F. Zhang, J. Vierock, O. Yizhar, L.E. Fenno, S. Tsunoda, A. Kianianmomeni, M. Prigge, A. Berndt, J. Cushman, J. Polle, J. Magnuson, P. Hegemann, K. Deisseroth, The microbial opsin family of optogenetic tools, Cell 147 (2011) 1446-1457.
[12] S.Y. Hou, E.G. Govorunova, M. Ntefidou, C.E. Lane, E.N. Spudich, O.A. Sineshchekov, J.L. Spudich, Diversity of *Chlamydomonas* channelrhodopsins, Photochem. Photobiol. 88 (2012) 119-128.
[13] L. Fenno, O. Yizhar, K. Deisseroth, The development and application of optogenetics, Annu. Rev. Neurosci. 34 (2011) 389-412.
[14] P. Hegemann, Algal sensory photoreceptors, Annu. Rev. Plant. Biol. 59 (2008) 167-189.
[15] J.L. Spudich, The multitalented microbial sensory rhodopsins, Trends Microbiol. 14 (2006) 480-487.
[16] O.A. Sineshchekov, K.H. Jung, J.L. Spudich, Two rhodopsins mediate phototaxis to low- and high-intensity light in *Chlamydomonas reinhardtii*, Proc. Natl. Acad. Sci. U. S. A. 99 (2002) 8689-8694.

[17] E.G. Govorunova, K.H. Jung, O.A. Sineshchekov, J.L. Spudich, *Chlamydomonas* sensory rhodopsins A and B: cellular content and role in photophobic responses, Biophys. J. 86 (2004) 2342-2349.
[18] P. Berthold, S.P. Tsunoda, O.P. Ernst, W. Mages, D. Gradmann, P. Hegemann, Channelrhodopsin-1 initiates phototaxis and photophobic responses in *Chlamydomonas* by immediate light-induced depolarization, Plant Cell 20 (2008) 1665-1677.
[19] A.K. Sharma, J.L. Spudich, W.F. Doolittle, Microbial rhodopsins: functional versatility and genetic mobility, Trends Microbiol. 14 (2006) 463-469.
[20] J.L. Spudich, C.S. Yang, K.H. Jung, E.N. Spudich, Retinylidene proteins: structures and functions from archaea to humans, Annu. Rev. Cell. Dev. Biol. 16 (2000) 365-392.
[21] P. Hegemann, Vision in microalgae, Planta 203 (1997) 265-274.
[22] S. Kateriya, G. Nagel, E. Barnberg, P. Hegemann, "Vision" in single-celled algae, News Physiol. Sci. 19 (2004) 133-137.
[23] J.Y. Lin, A user's guide to channelrhodopsin variants: features, limitations and future developments, Exp. Physiol. 96 (2010) 19-25.
[24] J. Mattis, K.M. Tye, E.A. Ferenczi, C. Ramakrishnan, D.J. O'Shea, R. Prakash, L.A. Gunaydin, M. Hyun, L.E. Fenno, V. Gradinaru, O. Yizhar, K. Deisseroth, Principles for applying optogenetic tools derived from direct comparative analysis of microbial opsins, Nat. Methods 9 (2012) 159-172.
[25] G. Nagel, M. Brauner, J.F. Liewald, N. Adeishvili, E. Bamberg, A. Gottschalk, Light activation of channelrhodopsin-2 in excitable cells of *Caenorhabditis elegans* triggers rapid behavioral responses, Curr. Biol. 15 (2005) 2279-2284.
[26] C. Bamann, T. Kirsch, G. Nagel, E. Bamberg, Spectral characteristics of the photocycle of channelrhodopsin-2 and its implication for channel function, J. Mol. Biol. 375 (2008) 686-694.
[27] A. Berndt, M. Prigge, D. Gradmann, P. Hegemann, Two open states with progressive proton selectivities in the branched channelrhodopsin-2 photocycle, Biophys. J. 98 (2010) 753-761.
[28] A.P. Plazzo, N. De Franceschi, F. Da Broi, F. Zonta, M.F. Sanasi, F. Filippini, M. Mongillo, Bioinformatic and mutational analysis of channelrhodopsin-2 protein cation-conducting pathway, J. Biol. Chem. 287 (2012) 4818-4825.
[29] J.Y. Lin, M.Z. Lin, P. Steinbach, R.Y. Tsien, Characterization of engineered channelrhodopsin variants with improved properties and kinetics, Biophys. J. 96 (2009) 1803-1814.
[30] F. Schneider, D. Gradmann, P. Hegemann, Ion selectivity and competition in channelrhodopsins, Biophys. J. 105 (2013) 91-100.
[31] K. Feldbauer, D. Zimmermann, V. Pintschovius, J. Spitz, C. Bamann, E. Bamberg, Channelrhodopsin-2 is a leaky proton pump, Proc. Natl. Acad. Sci. U. S. A. 106 (2009) 12317-12322.
[32] R. Richards, R.E. Dempski, Re-introduction of transmembrane serine residues reduce the minimum pore diameter of channelrhodopsin-2, PLoS One 7 (2012) e50018.

[33] S.P. Tsunoda, P. Hegemann, Glu 87 of channelrhodopsin-1 causes pH-dependent color tuning and fast photocurrent inactivation, Photochem. Photobiol. 85 (2009) 564-569.
[34] C. Bamann, G. Nagel, E. Bamberg, Microbial rhodopsins in the spotlight, Curr. Opin. Neurobiol. 20 (2010) 610-616.
[35] C.J. Law, P.C. Maloney, D.N. Wang, Ins and outs of major facilitator superfamily antiporters, Annu. Rev. Microbiol. 62 (2008) 289-305.
[36] O. Jardetzky, Simple allosteric model for membrane pumps, Nature 211 (1966) 969-970.
[37] D. Gradmann, A. Berndt, F. Schneider, P. Hegemann, Rectification of the channelrhodopsin early conductance, Biophys. J. 101 (2011) 1057-1068.
[38] H.C. Watanabe, K. Welke, D.J. Sindhikara, P. Hegemann, M. Elstner, Towards an understanding of channelrhodopsin function: simulations lead to novel insights of the channel mechanism, J. Mol. Biol. 425 (2013) 1795-1814.
[39] D.C. Gadsby, Ion channels versus ion pumps: the principal difference, in principle, Nat. Rev. Mol. Cell. Biol. 10 (2009) 344-352.
[40] E.K. Hoffmann, Anion transport systems in the plasma membrane of vertebrate cells, Biochim. Biophys. Acta. 864 (1986) 1-31.
[41] A. Accardi, C. Miller, Secondary active transport mediated by a prokaryotic homologue of ClC Cl^- channels, Nature 427 (2004) 803-807.
[42] H. Jayaram, A. Accardi, F. Wu, C. Williams, C. Miller, Ion permeation through a Cl^--selective channel designed from a CLC Cl^-/H^+ exchanger, Proc. Natl. Acad. Sci. U. S. A. 105 (2008) 11194-11199.
[43] L.J. DeFelice, T. Goswami, Transporters as channels, Annu. Rev. Physiol. 69 (2007) 87-112.
[44] M.S. Sonders, S.G. Amara, Channels in transporters, Curr. Opin. Neurobiol. 6 (1996) 294-302.
[45] M. Nack, I. Radu, B.J. Schultz, T. Resler, R. Schlesinger, A.N. Bondar, C. Del Val, S. Abbruzzetti, C. Viappiani, C. Bamann, E. Bamberg, J. Heberle, Kinetics of proton release and uptake by channelrhodopsin-2, FEBS Lett. 586 (2012) 1344-1348.
[46] S. Grzesiek, N.A. Dencher, Time-course and stoichiometry of light-induced proton release and uptake during the photocycle of bacteriorhodopsin, FEBS Lett 208 (1986) 337-342.
[47] V.A. Lórenz-Fonfría, T. Resler, N. Krause, M. Nack, M. Gossing, G. Fischer von Mollard, C. Bamann, E. Bamberg, R. Schlesinger, J. Heberle, Transient protonation changes in channelrhodopsin-2 and their relevance to channel gating, Proc. Natl. Acad. Sci. U. S. A. 110 (2013) E1273-1281.
[48] J. Lísal, M. Maduke, The ClC-0 chloride channel is a 'broken' Cl^-/H^+ antiporter, Nat. Struct. Mol. Biol. 15 (2008) 805-810.
[49] H.C. Watanabe, K. Welke, F. Schneider, S. Tsunoda, F. Zhang, K. Deisseroth, P. Hegemann, M. Elstner, Structural model of channelrhodopsin, J. Biol. Chem. 287 (2012) 7456-7466.
[50] T. Suzuki, K. Yamasaki, S. Fujita, K. Oda, M. Iseki, K. Yoshida, M. Watanabe, H. Daiyasu, H. Toh, E. Asamizu, S. Tabata, K. Miura, H. Fukuzawa, S. Nakamura, T.

Takahashi, Archaeal-type rhodopsins in *Chlamydomonas*: model structure and intracellular localization, Biochem. Biophys. Res. Commun. 301 (2003) 711-717.
[51] K. Eisenhauer, J. Kuhne, E. Ritter, A.E. Berndt, S. Wolf, E. Freier, F. Bartl, P. Hegemann, K. Gerwert, In channelrhodopsin-2 E90 is crucial for ion selectivity and is deprotonated during the photocycle, J. Biol. Chem. (2012).
[52] G. Nagel, T. Szellas, S. Kateriya, N. Adeishvili, P. Hegemann, E. Bamberg, Channelrhodopsins: directly light-gated cation channels, Biochem. Soc. Trans. 33 (2005) 863-866.
[53] K. Ruffert, B. Himmel, D. Lall, C. Bamann, E. Bamberg, H. Betz, V. Eulenburg, Glutamate residue 90 in the predicted transmembrane domain 2 is crucial for cation flux through channelrhodopsin 2, Biochem Biophys Res Commun 410 (2011) 737-743.
[54] H.E. Kato, F. Zhang, O. Yizhar, C. Ramakrishnan, T. Nishizawa, K. Hirata, J. Ito, Y. Aita, T. Tsukazaki, S. Hayashi, P. Hegemann, A.D. Maturana, R. Ishitani, K. Deisseroth, O. Nureki, Crystal structure of the channelrhodopsin light-gated cation channel, Nature 482 (2012) 369-374.
[55] M. Muller, C. Bamann, E. Bamberg, W. Kuhlbrandt, Projection structure of channelrhodopsin-2 at 6 Å resolution by electron crystallography, J. Mol. Biol. 414 (2011) 86-95.
[56] S. Subramaniam, T. Hirai, R. Henderson, From structure to mechanism: electron crystallographic studies of bacteriorhodopsin, Philos. Trans. R. Soc. Lond. A 360 (2002) 859-874.
[57] J. Hoffmann, L. Aslimovska, C. Bamann, C. Glaubitz, E. Bamberg, B. Brutschy, Studying the stoichiometries of membrane proteins by mass spectrometry: microbial rhodopsins and a potassium ion channel, Phys. Chem. Chem. Phys. 12 (2010) 3480-3485.
[58] T. Sattig, C. Rickert, E. Bamberg, H.J. Steinhoff, C. Bamann, Light-induced movement of the transmembrane helix B in channelrhodopsin-2, Angew. Chem. Int. Ed. Engl. 52 (2013) 9705-9708.
[59] N. Krause, C. Engelhard, J. Heberle, R. Schlesinger, R. Bittl, Structural differences between the closed and open states of channelrhodopsin-2 as observed by EPR spectroscopy, FEBS Lett. 587 (2013) 3309-3313.
[60] E. Ritter, K. Stehfest, A. Berndt, P. Hegemann, F.J. Bartl, Monitoring light-induced structural changes of Channelrhodopsin-2 by UV-visible and Fourier transform infrared spectroscopy, J. Biol. Chem. 283 (2008) 35033-35041.
[61] H. Li, A.D. Robertson, J.H. Jensen, Very fast empirical prediction and rationalization of protein pK_a values, Proteins 61 (2005) 704-721.
[62] M. Kamiya, H.E. Kato, R. Ishitani, O. Nureki, S. Hayashi, Structural and spectral characterizations of C1C2 channelrhodopsin and its mutants by molecular simulations, Chem. Phys. Lett. 556 (2013) 266-271.
[63] J.K. Lanyi, Proton transfers in the bacteriorhodopsin photocycle, Biochim. Biophys. Acta 1757 (2006) 1012-1018.

[64] H. Otto, T. Marti, M. Holz, T. Mogi, M. Lindau, H.G. Khorana, M.P. Heyn, Aspartic acid-96 is the internal proton donor in the reprotonation of the Schiff base of bacteriorhodopsin, Proc. Natl. Acad. Sci. U. S. A. 86 (1989) 9228-9232.
[65] Y. Sugiyama, H. Wang, T. Hikima, M. Sato, J. Kuroda, T. Takahashi, T. Ishizuka, H. Yawo, Photocurrent attenuation by a single polar-to-nonpolar point mutation of channelrhodopsin-2, Photochem. Photobiol. Sci. 8 (2009) 328-336.
[66] C. Bamann, R. Gueta, S. Kleinlogel, G. Nagel, E. Bamberg, Structural guidance of the photocycle of channelrhodopsin-2 by an interhelical hydrogen bond, Biochemistry 49 (2010) 267-278.
[67] A. Berndt, O. Yizhar, L.A. Gunaydin, P. Hegemann, K. Deisseroth, Bi-stable neural state switches, Nat. Neurosci. 12 (2009) 229-234.
[68] M. Nack, I. Radu, M. Gossing, C. Bamann, E. Bamberg, G.F. von Mollard, J. Heberle, The DC gate in Channelrhodopsin-2: crucial hydrogen bonding interaction between C128 and D156, Photochem. Photobiol. Sci. 9 (2010) 194-198.
[69] N.H. Joh, A. Min, S. Faham, J.P. Whitelegge, D. Yang, V.L. Woods, J.U. Bowie, Modest stabilization by most hydrogen-bonded side-chain interactions in membrane proteins, Nature 453 (2008) 1266-1270.
[70] A. Perálvarez-Marín, M. Márquez, J.L. Bourdelande, E. Querol, E. Padrós, Thr-90 plays a vital role in the structure and function of bacteriorhodopsin, J. Biol. Chem. 279 (2004) 16403-16409.
[71] B. Nie, J. Stutzman, A. Xie, A vibrational spectral maker for probing the hydrogen-bonding status of protonated Asp and Glu residues, Biophys. J. 88 (2005) 2833-2847.
[72] K. Takei, R. Takahashi, T. Noguchi, Correlation between the hydrogen-bond structures and the C=O stretching frequencies of carboxylic acids as studied by density functional theory calculations: theoretical basis for interpretation of infrared bands of carboxylic groups in proteins, J. Phys. Chem. B 112 (2008) 6725-6731.
[73] T. Wada, K. Shimono, T. Kikukawa, M. Hato, N. Shinya, S.Y. Kim, T. Kimura-Someya, M. Shirouzu, J. Tamogami, S. Miyauchi, K.H. Jung, N. Kamo, S. Yokoyama, Crystal structure of the eukaryotic light-driven proton-pumping rhodopsin, *Acetabularia* rhodopsin II, from marine alga, J. Mol. Biol. 411 (2011) 986-998.
[74] W.P. Burmeister, Structural changes in a cryo-cooled protein crystal owing to radiation damage, Acta Crystallogr. D Biol. Crystallogr. 56 (2000) 328-341.
[75] O. Carugo, K. Djinovic Carugo, When X-rays modify the protein structure: radiation damage at work, Trends Biochem. Sci. 30 (2005) 213-219.
[76] F. Garczarek, K. Gerwert, Polarized FTIR spectroscopy in conjunction with in situ H/D exchange reveals the orientation of protein internal carboxylic acids, J. Am. Chem. Soc. 128 (2006) 28-29.
[77] K. Welke, H.C. Watanabe, T. Wolter, M. Gaus, M. Elstner, QM/MM simulations of vibrational spectra of bacteriorhodopsin and channelrhodopsin-2, Phys. Chem. Chem. Phys. 15 (2013) 6651-6659.
[78] P. Zhou, F. Tian, F. Lv, Z. Shang, Geometric characteristics of hydrogen bonds involving sulfur atoms in proteins, Proteins 76 (2009) 151-163.

[79] M. Wanko, M. Hoffmann, T. Frauenheim, M. Elstner, Computational photochemistry of retinal proteins, J. Comput. Aided Mol. Des. 20 (2006) 511-518.
[80] G.G. Kochendoerfer, S.W. Lin, T.P. Sakmar, R.A. Mathies, How color visual pigments are tuned, Trends Biochem. Sci. 24 (1999) 300-305.
[81] O.S. Mironova, R.G. Efremov, B. Person, J. Heberle, I.L. Budyak, G. Büldt, R. Schlesinger, Functional characterization of sensory rhodopsin II from *Halobacterium salinarum* expressed in *Escherichia coli*, FEBS Lett. 579 (2005) 3147-3151.
[82] M. Nack, I. Radu, C. Bamann, E. Bamberg, J. Heberle, The retinal structure of channelrhodopsin-2 assessed by resonance Raman spectroscopy, FEBS Lett. 583 (2009) 3676-3680.
[83] T. Althaus, W. Eisfield, R. Lohrmann, M. Stockburger, Application of Raman spectroscopy to retinal proteins Isr. J. Chem. 35 (1995) 227-251.
[84] T. Takahashi, B. Yan, P. Mazur, F. Derguini, K. Nakanishi, J.L. Spudich, Color regulation in the archaebacterial phototaxis receptor phoborhodopsin (sensory rhodopsin II), Biochemistry 29 (1990) 8467-8474.
[85] B. Aton, A.G. Doukas, R.H. Callender, B. Becher, T.G. Ebrey, Resonance Raman studies of the purple membrane, Biochemistry 16 (1977) 2995-2999.
[86] L. Shi, S.R. Yoon, A.G. Bezerra, Jr., K.H. Jung, L.S. Brown, Cytoplasmic shuttling of protons in anabaena sensory rhodopsin: implications for signaling mechanism, J Mol Biol 358 (2006) 686-700.
[87] L. Zimányi, J.K. Lanyi, Fourier transform Raman study of retinal isomeric composition and equilibration in halorhodopsin, J. Phys. Chem. B 101 (1997) 1930-1933.
[88] S.O. Smith, J. Lugtenburg, R.A. Mathies, Determination of retinal chromophore structure in bacteriorhodopsin with resonance Raman spectroscopy, J. Membr. Biol. 85 (1985) 95-109.
[89] S.O. Smith, J.A. Pardoen, J. Lugtenburg, R.A. Mathies, Vibrationa analysis of the 13-*cis*-retinal chromophore in dark-adapted bacteriorhodopsin, J. Am. Chem. Soc. 91 (1987) 804-819.
[90] L. Vogeley, O.A. Sineshchekov, V.D. Trivedi, J. Sasaki, J.L. Spudich, H. Luecke, *Anabaena* sensory rhodopsin: a photochromic color sensor at 2.0 Å, Science 306 (2004) 1390-1393.
[91] L.A. Gunaydin, O. Yizhar, A. Berndt, V.S. Sohal, K. Deisseroth, P. Hegemann, Ultrafast optogenetic control, Nat. Neurosci. 13 (2010) 387-392.
[92] P. Hildebrandt, M. Stockburger, Role of water in bacteriorhodopsin's chromophore: resonance Raman-study, Biochemistry 23 (1984) 5539-5548.
[93] H. Luecke, B. Schobert, H.T. Richter, J.P. Cartailler, J.K. Lanyi, Structure of bacteriorhodopsin at 1.55 Å resolution, J. Mol. Biol. 291 (1999) 899-911.
[94] O.P. Ernst, P.A. Sánchez Murcia, P. Daldrop, S.P. Tsunoda, S. Kateriya, P. Hegemann, Photoactivation of channelrhodopsin, J. Biol. Chem. 283 (2008) 1637-1643.
[95] J.P. Klare, I. Chizhov, M. Engelhard, Microbial rhodopsins: scaffolds for ion pumps, channels, and sensors, Results Probl. Cell Differ. 45 (2008) 73-122.

[96] J.K. Lanyi, G. Váró, The photocycles of bacteriorhodopsin, Isr. J. Chem. 35 (1995) 365-385.
[97] O.A. Sineshchekov, E.G. Govorunova, J. Wang, H. Li, J.L. Spudich, Intramolecular proton transfer in channelrhodopsins, Biophys. J. 104 (2013) 807-817.
[98] A. Berndt, P. Schoenenberger, J. Mattis, K.M. Tye, K. Deisseroth, P. Hegemann, T.G. Oertner, High-efficiency channelrhodopsins for fast neuronal stimulation at low light levels, Proc. Natl. Acad. Sci. U. S. A. 108 (2011) 7595-7600.
[99] S. Kleinlogel, K. Feldbauer, R.E. Dempski, H. Fotis, P.G. Wood, C. Bamann, E. Bamberg, Ultra light-sensitive and fast neuronal activation with the Ca^{2+}-permeable channelrhodopsin CatCh, Nat. Neurosci. 14 (2011) 513-518.
[100] K. Stehfest, E. Ritter, A. Berndt, F. Bartl, P. Hegemann, The branched photocycle of the slow-cycling channelrhodopsin-2 mutant C128T, J. Mol. Biol. 398 (2010) 690-702.
[101] K. Stehfest, P. Hegemann, Evolution of the channelrhodopsin photocycle model, Chemphyschem 11 (2010) 1120-1126.
[102] M.K. Verhoefen, C. Bamann, R. Blocher, U. Förster, E. Bamberg, J. Wachtveitl, The photocycle of channelrhodopsin-2: ultrafast reaction dynamics and subsequent reaction steps, Chemphyschem 11 (2010) 3113-3122.
[103] M.K. Neumann-Verhoefen, K. Neumann, C. Bamann, I. Radu, J. Heberle, E. Bamberg, J.L. Wachtveitl, Ultrafast infrared spectroscopy on channelrhodopsin-2 reveals efficient energy transfer from the retinal chromophore to the protein, J. Am. Chem. Soc. 35 (2013) 6968–6976.
[104] F. Scholz, E. Bamberg, C. Bamann, J. Wachtveitl, Tuning the primary reaction of channelrhodopsin-2 by imidazole, pH, and site-specific mutations, Biophys. J. 102 (2012) 2649-2657.
[105] I. Radu, C. Bamann, M. Nack, G. Nagel, E. Bamberg, J. Heberle, Conformational changes of channelrhodopsin-2, J. Am. Chem. Soc. 131 (2009) 7313-7319.
[106] X. Jiang, E. Zaitseva, M. Schmidt, F. Siebert, M. Engelhard, R. Schlesinger, K. Ataka, R. Vogel, J. Heberle, Resolving voltage-dependent structural changes of a membrane photoreceptor by surface-enhanced IR difference spectroscopy, Proc. Natl. Acad. Sci. U. S. A. 105 (2008) 12113-12117.
[107] K. Nikolic, N. Grossman, M.S. Grubb, J. Burrone, C. Toumazou, P. Degenaar, Photocycles of channelrhodopsin-2, Photochem. Photobiol. 85 (2009) 400-411.
[108] S.P. Balashov, Photoreactions of the photointermediates of bacteriorhodopsin, Isr. J. Chem. 35 (1995) 415-428.
[109] S. Druckmann, N. Friedman, J.K. Lanyi, R. Needleman, M. Ottolenghi, M. Sheves, The back photoreaction of the M intermediate in the photocycle of bacteriorhodopsin: mechanism and evidence for two M species, Photochem. Photobiol. 56 (1992) 1041-1047.
[110] S. Bruun, H. Naumann, U. Kuhlmann, C. Schulz, K. Stehfest, P. Hegemann, P. Hildebrandt, The chromophore structure of the long-lived intermediate of the C128T channelrhodopsin-2 variant, FEBS Lett 585 (2011) 3998-4001.

[111] P. Hegemann, A. Moglich, Channelrhodopsin engineering and exploration of new optogenetic tools, Nat. Methods 8 (2011) 39-42.
[112] G.S. Harbison, S.O. Smith, J.A. Pardoen, C. Winkel, J. Lugtenburg, J. Herzfeld, R. Mathies, R.G. Griffin, Dark-adapted bacteriorhodopsin contains 13-*cis*, 15-*syn* and all-*trans*, 15-*anti* retinal Schiff bases, Proc. Natl. Acad. Sci. U. S. A. 81 (1984) 1706-1709.
[113] M.J. Pettei, A.P. Yudd, K. Nakanishi, R. Henselman, W. Stoeckenius, Identification of retinal isomers isolated from bacteriorhodopsin, Biochemistry 16 (1977) 1955-1959.
[114] P. Hegemann, S. Ehlenbeck, D. Gradmann, Multiple photocycles of channelrhodopsin, Biophys. J. 89 (2005) 3911-3918.
[115] J.C. Williams, J. Xu, Z. Lu, A. Klimas, X. Chen, C.M. Ambrosi, I.S. Cohen, E. Entcheva, Computational optogenetics: empirically-derived voltage- and light-sensitive channelrhodopsin-2 model, PLoS Comput. Biol. 9 (2013) e1003220.
[116] R.A. Stefanescu, R.G. Shivakeshavan, P.P. Khargonekar, S.S. Talathi, Computational modeling of channelrhodopsin-2 photocurrent characteristics in relation to neural signaling, Bull. Math. Biol. (2013).
[117] E. Ritter, P. Piwowarski, P. Hegemann, F.J. Bartl, Light-dark adaptation of Channelrhodopsin C128T mutant, J. Biol. Chem. (2013).
[118] G. Váró, L. Zimányi, X. Fan, L. Sun, R. Needleman, J.K. Lanyi, Photocycle of halorhodopsin from *Halobacterium salinarium*, Biophys. J. 68 (1995) 2062-2072.
[119] C. Gergely, C. Ganea, G. Váró, Combined optical and photoelectric study of the photocycle of 13-*cis* bacteriorhodopsin, Biophys J 67 (1994) 855-861.
[120] L. Shi, S.R. Yoon, A.G. Bezerra, Jr., K.H. Jung, L.S. Brown, Cytoplasmic shuttling of protons in anabaena sensory rhodopsin: implications for signaling mechanism, J. Mol. Biol. 358 (2006) 686-700.
[121] E. Goormaghtigh, V. Cabiaux, J.M. Ruysschaert, Determination of soluble and membrane protein structure by Fourier transform infrared spectroscopy. I. Assignments and model compounds, Subcell. Biochem. 23 (1994) 329-362.
[122] A. Maeda, Application of FTIR spectroscopy to the structural study on the function of bacteriorhodopsin, Isr. J. Chem. 35 (1995) 387-400.
[123] R.E. Martin, M. Pannier, F. Diederich, V. Gramlich, M. Hubrich, H.W. Spiess, Determination of end-to-end distances in a series of TEMPO diradicals of up to 2.8 nm length with a new four-pulse double electron electron resonance experiment, Angew. Chem. Int. Ed. 37 (1998) 2834-2837.
[124] C. Altenbach, A.K. Kusnetzow, O.P. Ernst, K.P. Hofmann, W.L. Hubbell, High-resolution distance mapping in rhodopsin reveals the pattern of helix movement due to activation, Proc. Natl. Acad. Sci. U. S. A. 105 (2008) 7439-7444.
[125] S. Krimm, J. Bandekar, Vibrational spectroscopy and conformation of peptides, polypeptides, and proteins, Adv. Protein. Chem. 3 (1986) 181-364.
[126] E. Goormaghtigh, V. Cabiaux, J.M. Ruysschaert, Determination of soluble and membrane protein structure by Fourier transform infrared spectroscopy. III. Secondary structures, Subcell. Biochem. 23 (1994) 405-450.

[127] M. Grechko, M.T. Zanni, Quantification of transition dipole strengths using 1D and 2D spectroscopy for the identification of molecular structures via exciton delocalization: application to α-helices, J. Chem. Phys. 137 (2012) 184202.
[128] K. Gerwert, F. Siebert, Evidence for light-induced 13-*cis*, 14-s-*cis* isomerization in bacteriorhodopsin obtained by FTIR difference spectroscopy using isotopically labelled retinals, EMBO J. 5 (1986) 805-811.
[129] A.K. Dioumaev, Infrared methods for monitoring the protonation state of carboxylic amino acids in the photocycle of bacteriorhodopsin, Biochemistry (Mosc) 66 (2001) 1269-1276.
[130] A. Barth, The infrared absorption of amino acid side chains, Prog. Biophys. Mol. Biol. 74 (2000) 141-173.
[131] M.S. Braiman, T. Mogi, T. Marti, L.J. Stern, H.G. Khorana, K.J. Rothschild, Vibrational spectroscopy of bacteriorhodopsin mutants: light-driven proton transport involves protonation changes of aspartic acid residues 85, 96, and 212, Biochemistry 27 (1988) 8516-8520.
[132] J. Heberle, D. Oesterhelt, N.A. Dencher, Decoupling of photo- and proton cycle in the Asp85→Glu mutant of bacteriorhodopsin, EMBO J. 12 (1993) 3721-3727.
[133] H. Otto, T. Marti, M. Holz, T. Mogi, L.J. Stern, F. Engel, H.G. Khorana, M.P. Heyn, Substitution of amino acids Asp-85, Asp-212, and Arg-82 in bacteriorhodopsin affects the proton release phase of the pump and the pK of the Schiff base, Proc. Natl. Acad. Sci. U. S. A. 87 (1990) 1018-1022.
[134] M. Kataoka, H. Kamikubo, F. Tokunaga, L.S. Brown, Y. Yamazaki, A. Maeda, M. Sheves, R. Needleman, J.K. Lanyi, Energy coupling in an ion pump. The reprotonation switch of bacteriorhodopsin, J. Mol. Biol. 243 (1994) 621-638.
[135] G. Iliadis, G. Zundel, B. Brzezinski, Aspartic proteinases – Fourier transform IR studies of the aspartic carboxylic groups in the active site of pepsin, FEBS Lett. 352 (1994) 315-317.
[136] A.K. Dioumaev, H.T. Richter, L.S. Brown, M. Tanio, S. Tuzi, H. Saitô, Y. Kimura, R. Needleman, J.K. Lanyi, Existence of a proton transfer chain in bacteriorhodopsin: Participation of Glu-194 in the release of protons to the extracellular surface, Biochemistry 37 (1998) 2496-2506.
[137] S. Wolf, E. Freier, M. Potschies, E. Hofmann, K. Gerwert, Directional proton transfer in membrane proteins achieved through protonated protein-bound water molecules: a proton diode, Angew. Chem. Int. Ed. Engl. 49 (2010) 6889-6893.
[138] L.S. Brown, J. Sasaki, H. Kandori, A. Maeda, R. Needleman, J.K. Lanyi, Glutamic acid 204 is the terminal proton release group at the extracellular surface of bacteriorhodopsin, J. Biol. Chem. 270 (1995) 27122-27126.
[139] P. Phatak, N. Ghosh, H. Yu, Q. Cui, M. Elstner, Amino acids with an intermolecular proton bond as proton storage site in bacteriorhodopsin, Proc. Natl. Acad. Sci. U.S.A. 105 (2008) 19672-19677.
[140] A.K. Dioumaev, L.S. Brown, R. Needleman, J.K. Lanyi, Fourier transform infrared spectra of a late intermediate of the bacteriorhodopsin photocycle suggest transient protonation of Asp-212, Biochemistry 38 (1999) 10070-10078.

[141] C. Zscherp, J. Heberle, Infrared difference spectra of the intermediates L, M, N, and O of the bacteriorhodopsin photoreaction obtained by time-resolved attenuated total reflection spectroscopy, J. Phys. Chem. B 101 (1997) 10542-10547.
[142] C. Zscherp, R. Schlesinger, J. Heberle, Time-resolved FT-IR spectroscopic investigation of the pH-dependent proton transfer reactions in the E194Q mutant of bacteriorhodopsin, Biochem. Biophys. Res. Commun. 283 (2001) 57-63.
[143] P. Phatak, J.S. Frähmcke, M. Wanko, M. Hoffmann, P. Strodel, J.C. Smith, S. Suhai, A.N. Bondar, M. Elstner, Long-distance proton transfer with a break in the bacteriorhodopsin active site, J. Am. Chem. Soc. 131 (2009) 7064-7078.
[144] A.K. Dioumaev, L.S. Brown, J. Shih, E.N. Spudich, J.L. Spudich, J.K. Lanyi, Proton transfers in the photochemical reaction cycle of proteorhodopsin, Biochemistry 41 (2002) 5348-5358.
[145] M.R. Miranda, A.R. Choi, L. Shi, A.G. Bezerra, Jr., K.H. Jung, L.S. Brown, The photocycle and proton translocation pathway in a cyanobacterial ion-pumping rhodopsin, Biophys. J. 96 (2009) 1471-1481.
[146] J. Tittor, C. Soell, D. Oesterhelt, H.J. Butt, E. Bamberg, A defective proton pump, point-mutated bacteriorhodopsin Asp96 → Asn is fully reactivated by azide, EMBO J. 8 (1989) 3477-3482.
[147] G. Metz, F. Siebert, M. Engelhard, Asp^{85} Is the only internal aspartic-acid that gets protonated in the M-Intermediate and the purple-to-blue transition of bacteriorhodopsin - a solid-state ^{13}C CP-MAS NMR investigation, FEBS Lett. 303 (1992) 237-241.
[148] A. Perálvarez-Marín, V.A. Lórenz-Fonfría, J.-L. Bourdelande, E. Querol, H. Kandori, E. Padrós, Inter-helical hydrogen bonds are essential elements for intra-protein signal transduction: the role of Asp115 in bacteriorhodopsin transport function, J. Mol. Biol. 368 (2007) 666-676.
[149] E. Bombarda, T. Becker, G.M. Ullmann, Influence of the membrane potential on the protonation of bacteriorhodopsin: insights from electrostatic calculations into the regulation of proton pumping, J. Am. Chem. Soc. 128 (2006) 12129-12139.
[150] J. Tittor, M. Wahl, U. Schweiger, D. Oesterhelt, Specific acceleration of deprotonation and reprotonation steps by azide in mutated bacteriorhodopsins, Biochim. Biophys. Acta. 1187 (1994) 191-197.
[151] R. Simon-Vazquez, M. Dominguez, V.A. Lorenz-Fonfria, S. Alvarez, J.L. Bourdelande, A.R. de Lera, E. Padros, A. Peralvarez-Marin, Probing a polar cluster in the retinal binding pocket of bacteriorhodopsin by a chemical design approach, PLoS One 7 (2012) e42447.
[152] F. Garczarek, L.S. Brown, J.K. Lanyi, K. Gerwert, Proton binding within a membrane protein by a protonated water cluster, Proc. Natl. Acad. Sci. U S A 102 (2005) 3633-3638.
[153] R. Rammelsberg, G. Huhn, M. Lübben, K. Gerwert, Bacteriorhodopsin's intramolecular proton-release pathway consists of a hydrogen-bonded network, Biochemistry 37 (1998) 5001-5009.
[154] S.P. Balashov, Protonation reactions and their coupling in bacteriorhodopsin, Biochim. Biophys. Acta. 1460 (2000) 75-94.

[155] A. Wand, I. Gdor, J. Zhu, M. Sheves, S. Ruhman, Shedding new light on retinal protein photochemistry, Annu. Rev. Phys. Chem. 64 (2013) 437-458.
[156] N. Mizuide, M. Shibata, N. Friedman, M. Sheves, M. Belenky, J. Herzfeld, H. Kandori, Structural changes in bacteriorhodopsin following retinal photoisomerization from the 13-*cis* form, Biochemistry 45 (2006) 10674-10681.
[157] A. Kawanabe, Y. Furutani, K.H. Jung, H. Kandori, FTIR study of the photoisomerization processes in the 13-*cis* and all-*trans* forms of *Anabaena* sensory rhodopsin at 77 K, Biochemistry 45 (2006) 4362-4370.
[158] J. Hofrichter, E.R. Henry, R.H. Lozier, Photocycles of bacteriorhodopsin in light- and dark-adapted purple membrane studied by time-resolved absorption spectroscopy, Biophys. J. 56 (1989) 693-706.
[159] L.A. Drachev, S.V. Dracheva, A.D. Kaulen, pH dependence of the formation of an M-type intermediate in the photocycle of 13-*cis*-bacteriorhodopsin, FEBS Lett. 332 (1993) 67-70.
[160] G. Steinberg, M. Sheves, S. Bressler, M. Ottolenghi, Factors affecting the formation of an M-like intermediate in the photocycle of 13-*cis*-bacteriorhodopsin, Biochemistry 33 (1994) 12439-12450.
[161] I. Logunov, W. Humphrey, K. Schulten, M. Sheves, Molecular dynamics study of the 13-*cis* form (bR_{548}) of bacteriorhodopsin and its photocycle, Biophys. J. 68 (1995) 1270-1282.
[162] W. Stoeckenius, Bacterial rhodopsins: evolution of a mechanistic model for the ion pumps, Protein. Sci. 8 (1999) 447-459.
[163] M. Grote, M. Engelhard, P. Hegemann, Of ion pumps, sensors and channels - Perspectives on microbial rhodopsins between science and history, Biochim. Biophys. Acta (2013).
[164] J.L. Spudich, O.A. Sineshchekov, E.G. Govorunova, Mechanism divergence in microbial rhodopsins, Biochim. Biophys. Acta (2013).
[165] C. Del Val, J. Royuela-Flor, S. Milenkovic, A.N. Bondar, Channelrhodopsins: a bioinformatics perspective, Biochim. Biophys. Acta (2013).
[166] X. Jiang, M. Engelhard, K. Ataka, J. Heberle, Molecular impact of the membrane potential on the regulatory mechanism of proton transfer in sensory rhodopsin II, J. Am. Chem. Soc. 132 (2010) 10808-10815.
[167] S. Geibel, T. Friedrich, P. Ormos, P.G. Wood, G. Nagel, E. Bamberg, The voltage-dependent proton pumping in bacteriorhodopsin is characterized by optoelectric behavior, Biophys. J. 81 (2001) 2059-2068.
[168] L. Rivas, S. Hippler-Mreyen, M. Engelhard, P. Hildebrandt, Electric-field dependent decays of two spectroscopically different M-states of photosensory rhodopsin II from *Natronobacterium pharaonis*, Biophys. J. 84 (2003) 3864-3873.
[169] Y. Furutani, H. Kandori, Hydrogen-bonding changes of internal water molecules upon the actions of microbial rhodopsins studied by FTIR spectroscopy, Biochim. Biophys. Acta (2013).
[170] K. Gerwert, E. Freier, S. Wolf, The role of protein-bound water molecules in microbial rhodopsins, Biochim. Biophys. Acta (2013).

[171] R. Efremov, V.I. Gordeliy, J. Heberle, G. Büldt, Time-resolved microspectroscopy on a single crystal of bacteriorhodopsin reveals lattice-induced differences in the photocycle kinetics, Biophys. J. 91 (2006) 1441-1451.
[172] R. Moukhametzianov, J.P. Klare, R. Efremov, C. Baeken, A. Goppner, J. Labahn, M. Engelhard, G. Buldt, V.I. Gordeliy, Development of the signal in sensory rhodopsin and its transfer to the cognate transducer, Nature 440 (2006) 115-119.
[173] U. Alexiev, D.L. Farrens, Fluorescence spectroscopy of rhodopsins: Insights and approaches, Biochim. Biophys. Acta (2013).
[174] A. Aquila, M.S. Hunter, R.B. Doak, R.A. Kirian, P. Fromme, T.A. White, J. Andreasson, D. Arnlund, S. Bajt, T.R.M. Barends, M. Barthelmess, M.J. Bogan, C. Bostedt, H. Bottin, J.D. Bozek, C. Caleman, N. Coppola, J. Davidsson, D.P. DePonte, V. Elser, S.W. Epp, B. Erk, H. Fleckenstein, L. Foucar, M. Frank, R. Fromme, H. Graafsma, I. Grotjohann, L. Gumprecht, J. Hajdu, C.Y. Hampton, A. Hartmann, R. Hartmann, S. Hauriege, G. Hauser, H. Hirsemann, P. Holl, J.M. Holton, A. Homke, L. Johansson, N. Kimmel, S. Kassemeyer, F. Krasniqi, K. Kuhnel, M.N. Liang, L. Lomb, E. Malmerberg, S. Marchesini, A.V. Martin, F.R.N.C. Maia, M. Messerschmidt, K. Nass, C. Reich, R. Neutze, D. Rolles, B. Rudek, A. Rudenko, I. Schlichting, C. Schmidt, K.E. Schmidt, J. Schulz, M.M. Seibert, R.L. Shoeman, R. Sierra, H. Soltau, D. Starodub, F. Stellato, S. Stern, L. Struder, N. Timneanu, J. Ullrich, X.Y. Wang, G.J. Williams, G. Weidenspointner, U. Weierstall, C. Wunderer, A. Barty, J.C.H. Spence, H.N. Chapman, Time-resolved protein nanocrystallography using an X-ray free-electron laser, Opt. Express 20 (2012) 2706-2716.
[175] R. Neutze, K. Moffat, Time-resolved structural studies at synchrotrons and X-ray free electron lasers: opportunities and challenges, Curr. Opin. Struc. Biol. 22 (2012) 651-659.
[176] A. Yurtsever, A.H. Zewail, 4D nanoscale diffraction observed by convergent-beam ultrafast electron microscopy, Science 326 (2009) 708-712.
[177] G. Sciaini, R.J.D. Miller, Femtosecond electron diffraction: heralding the era of atomically resolved dynamics, Rep. Prog. Phys. 74 (2011).
[178] H. Kandori, Role of internal water molecules in bacteriorhodopsin, Biochim. Biophys. Acta 1460 (2000) 177-191.
[179] V.A. Lórenz-Fonfría, Y. Furutani, T. Ota, K. Ido, H. Kandori, Protein fluctuations as the possible origin of the thermal activation of rod photoreceptors in the dark, J. Am. Chem. Soc. 132 (2010) 5693-5703.

Figure captions

Figure 1. Structural models of ChR2. (a) Ribbon representation of the X-ray crystallographic structure of the ChR1-ChR2 (C1C2) chimera (pdb entry: 3UGA, [54]). Helices A–E are shown in dark yellow, which correspond to the amino acid sequence of ChR1. Helices F and G are shown in purple, which correspond to residues derived from ChR2. The left graph represents the in-plane view to the membrane, showing the helices and sheets including water molecules (green spheres) and the retinal linked to a lysine residue in the middle of the membrane. In the right graph, the molecule is rotated by 90° for a view perpendicular to the membrane plane. (b) Transmembrane segments of helices A, B, C, and G are shown that frame the putative cation pathway in the C1C2 chimera with some relevant residues. The residue numbering corresponds to ChR2. (c) Hydrogen-bonding interactions of the side chains of D156 and C128 (DC gate). (d) Absorption spectrum of the retinal in ChR2 (black trace). Note its characteristic fine structure (dashed vertical lines), resolved in the second derivative spectrum (red trace). (e) Chromatogram of the chemically extracted retinal from dark-state ChR2. The peaks are assigned to different retinal isomers based on their characteristic retention time.

Figure 2. Light response and photocycle of ChR2 under single turnover conditions (nanosecond blue light excitation). (a) Photocurrents of ChR2 for two different membrane potentials. Kinetic traces are plotted on a logarithmic time scale. ChR2 was expressed in HEK cells and the current was measured by patch clamp in a whole-cell configuration at room temperature [26]. (b) Transient absorption changes of ChR2 solubilised in detergent, at 25 ^{o}C and pH 7.4 [47]. Positive absorption (yellow to red) reports the formation of intermediate states with a λ_{max} differing from the ground state, namely, P_1^{500}, P_2^{390}, P_3^{520}, and P_4^{480} (the superscripts indicate the λ_{max} for each intermediate). The negative absorption (blue) corresponds to the depletion of the dark state. The sequence of interconversions between intermediates is indicated by solid arrows. The dark-state recovery tallies P_3^{520} decay (dashed

arrow). (c) Simplified uni-directional photocycle model of ChR2, including half-lives. Possible branches and back reactions are ignored.

Figure 3. Photocurrent response and photocycle of ChR2 under continuous illumination. (a) Illustrative (synthetic) photocurrent of ChR2 expressed in a host cell under negative voltage-clamp conditions and rectangular blue light excitation (blue bars). After an initial peak, I_p, the photocurrent decays (desensitises) to a steady state, I_{ss}, and relaxes to zero when the light is switched off. A second pulse after a certain time delay, Δt, generates a smaller peak current (light adaptation). (b) Four-state model used to describe the photocurrents under continuous illumination (adapted from Hegemann *et al.* [114] and Nikolic *et al.* [107]). The model includes two closed states (C1 and C2) and two open conductive states (O1 and O2). Approximate time constants are indicated for thermally driven transitions (plain arrows). Light-driven transitions (wavy arrows) depend on, among other factors, wavelength and intensity.

Figure 4. Light-induced FTIR difference spectra at 80 K for ChR2 [68], light-adapted bacteriorhodopsin (bR [178]), and bovine visual rhodopsin (Rho [179]). Typical wavenumber regions are indicated by horizontal bars for vibrations of the protein backbone (amide I and II vibrations, mainly C=O stretching and C=N strecth coupled to N-H bending vibrations, respectively), amino acid side chains (carboxylic group $_{\nu}$C=O of Asp and Glu), the Schiff base ($_{\nu}$C=N), and retinal ($_{\nu}$C=C and $_{\nu}$C-C stretching vibrations). The spectra were normalised to the intensities of bands of the C-C stretching vibrations of retinal. Of particular note are the strong intensities of the amide I bands of ChR2.

Figure 5. Schematic representation of the photocycle of ChR2. Proton transfer reactions as well as conformational changes of the apoprotein and the retinal chromophore are depicted that constitute the transitions between intermediate states. The proton transfer reactions are colour coded and overlaid on the structural model of the C1C2 chimera (pdb 3UGA) [54]. PRG corresponds to the putative proton

release group. The photocycle starts from the initial dark state (ChR2) by light-induced retinal isomerisation from all-*trans* (AT) to 13-*cis*, accompanied by conformational changes in transmembrane helices. The channel opens in between two P_2^{390} substates, closes in the subsequent P_3^{520} to ChR2 transition, and is desensitised in the P_3^{520} to P_4^{480} transition.

Figure 1

Click here to download high resolution image

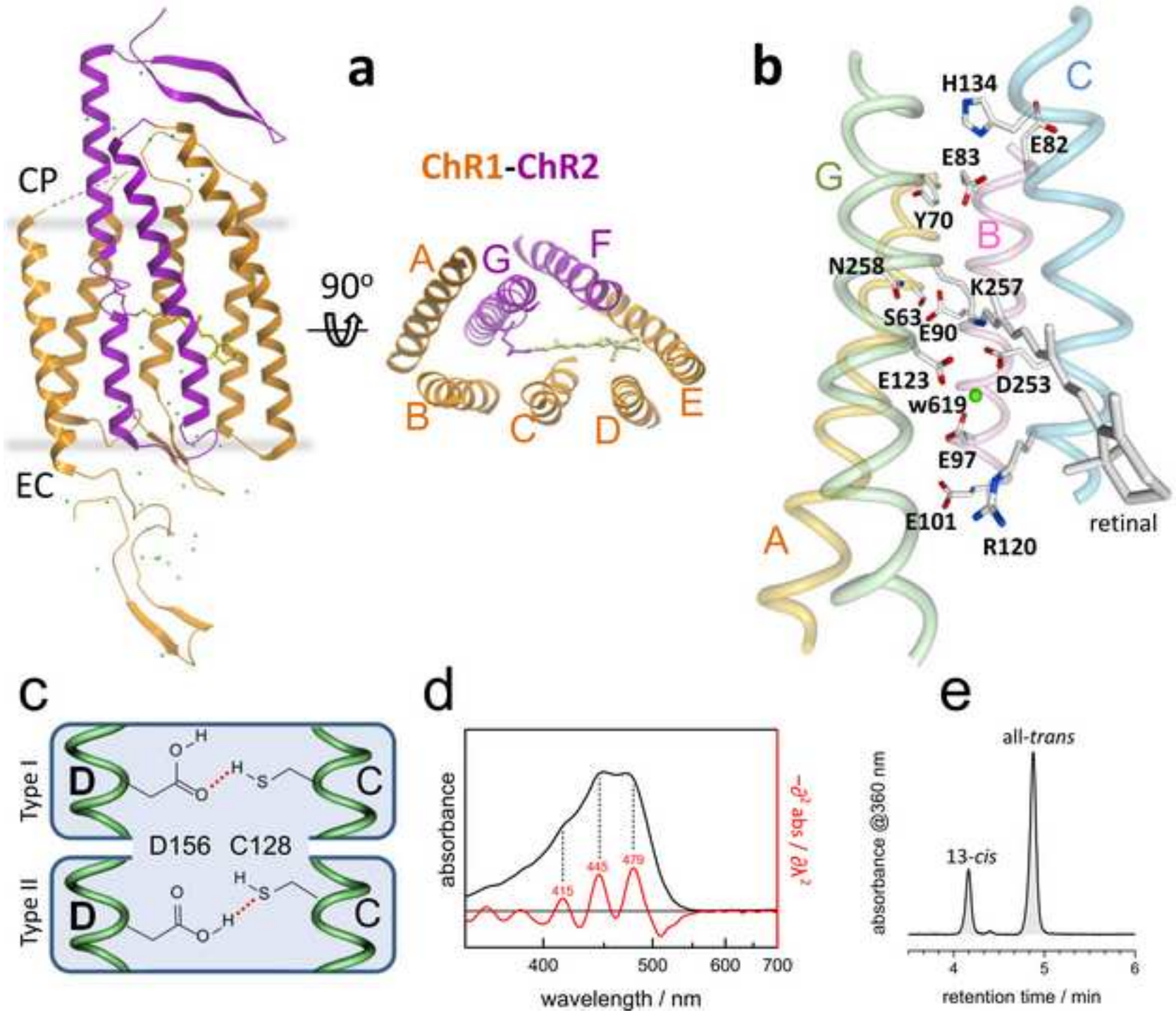

Figure 2

Click here to download high resolution image

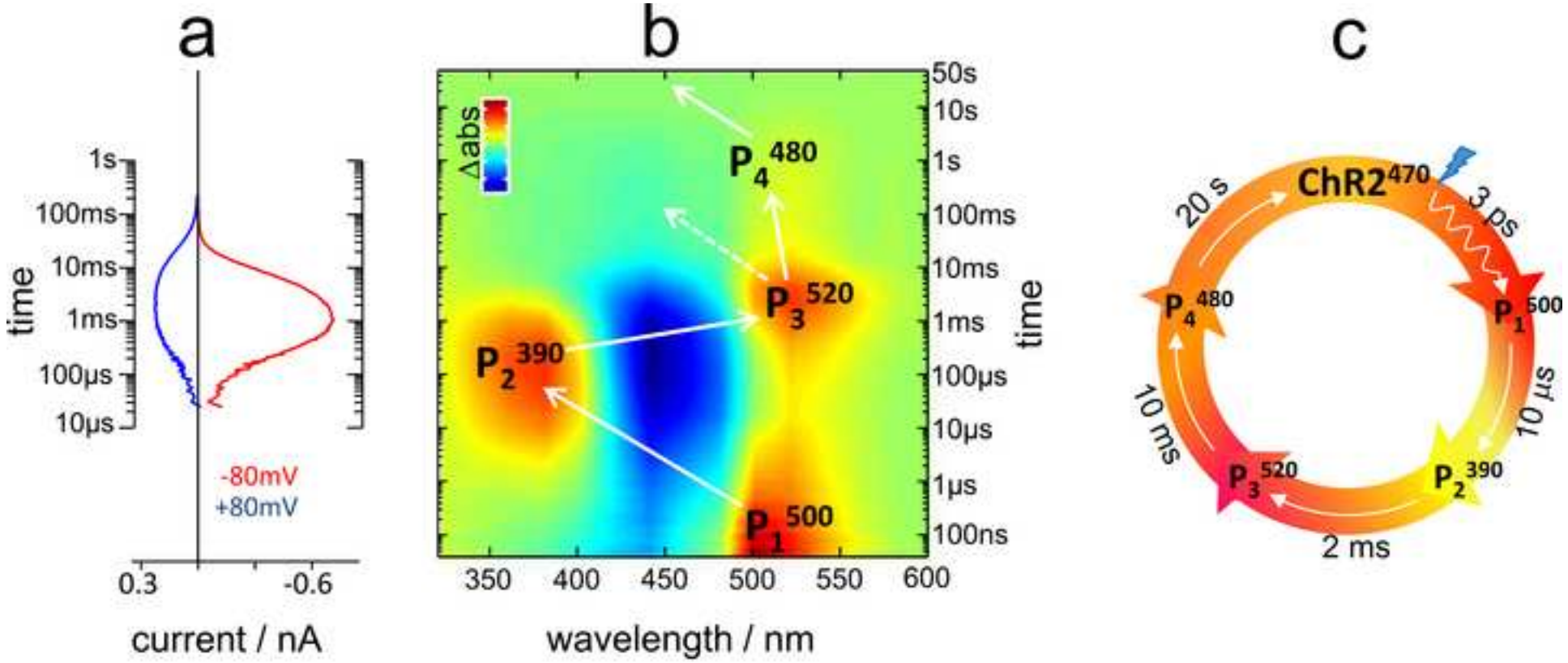

Figure 3

Click here to download high resolution image

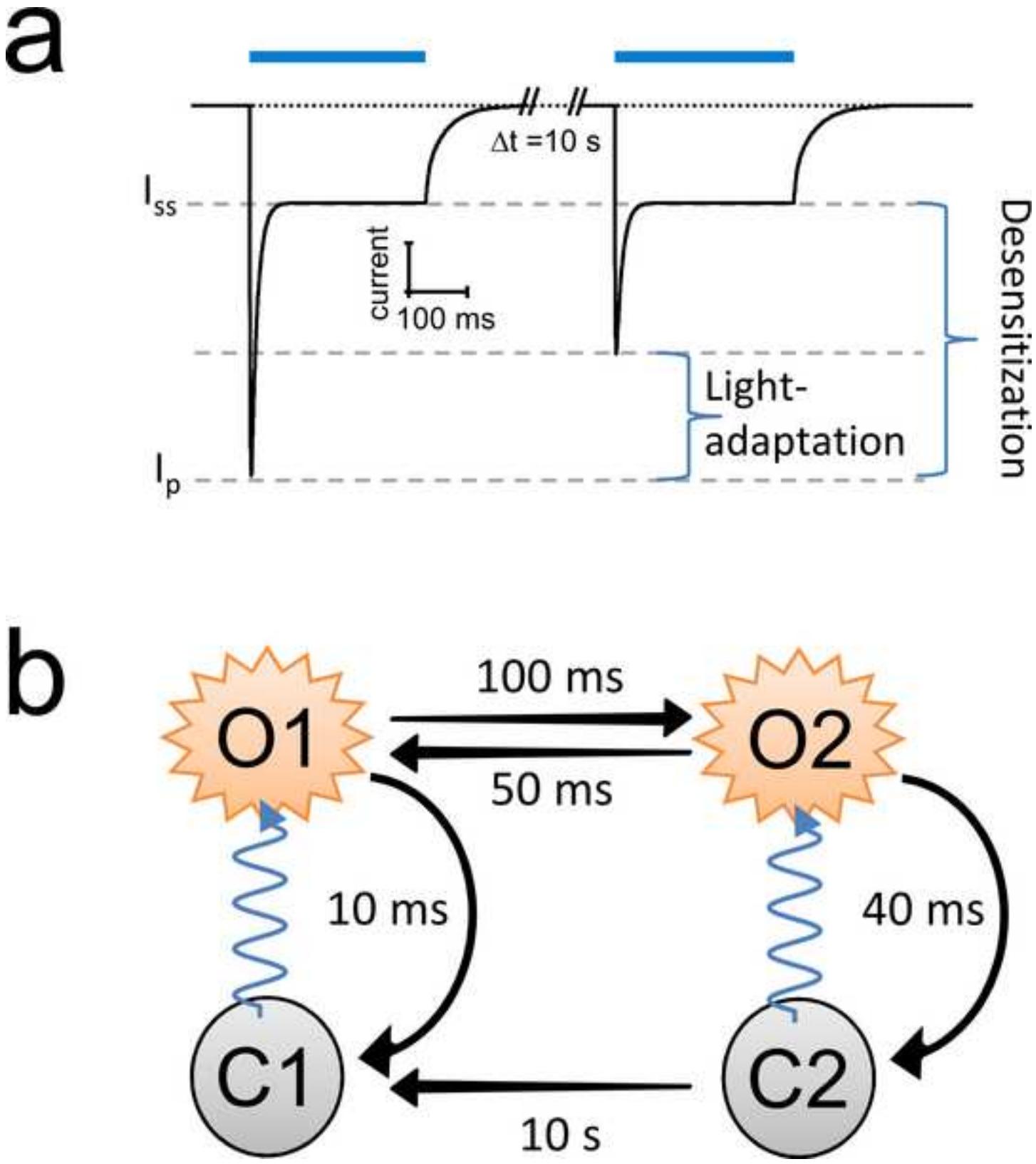

Figure 4

Click here to download high resolution image

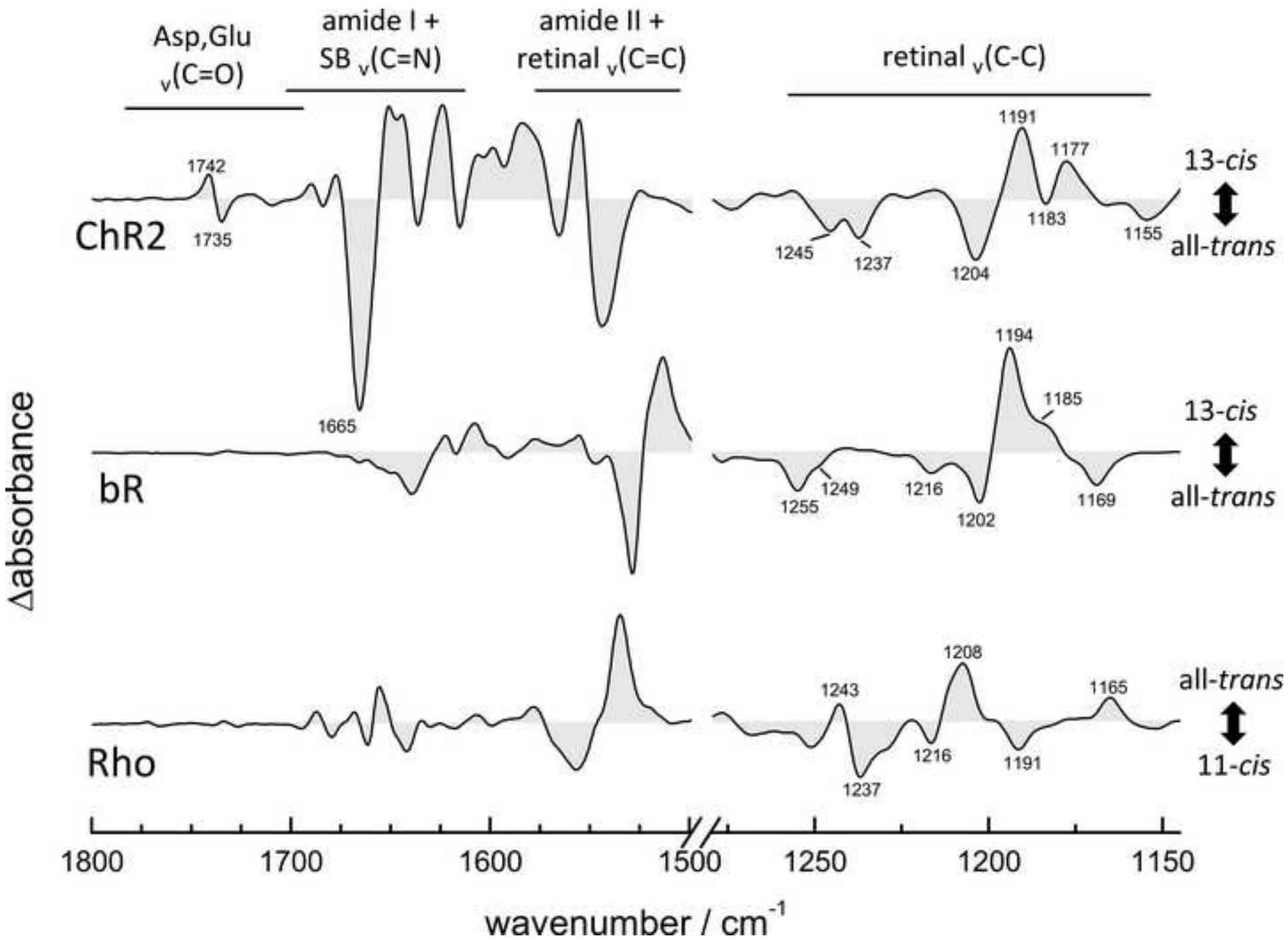

Figure 5

Click here to download high resolution image